EXTRACTING THE ROTATIONAL DEGREES OF FREEDOM FROM RECONSTRUCTED THREE-DIMENSIONAL VELOCITY FIELDS

by
James Raymond DeVlaminck II

Thesis submitted to the Faculty of the
Virginia Polytechnic Institute and State University
in partial fulfillment of the requirements for the degree of

Masters of Science
in
Mechanical Engineering

L. D. Mitchell, Chairman
R. L. West
D. J. Leo

July 16, 2001
Blacksburg, Virginia

Keywords: Vibration, Laser Doppler Velocimetry, Angular Velocity

EXTRACTING THE ROTATIONAL DEGREES OF FREEDOM FROM A RECONSTRUCTED THREE-DIMENSIONAL VELOCITY FIELD ALONG WITH AN ANALYTICAL DEMONSTRATON AND A PROPOSED METHOD FOR EXPERIMENTAL VERIFICATION

by

James Raymond DeVlaminck II

Committee Chairman: L. D. Mitchell
Mechanical Engineering

(ABSTRACT)

A theoretical method for extracting the rotational degrees of freedom from a reconstructed three-dimensional velocity field has been developed. To extract the angular velocities the curl of the translational velocities must be performed. The three-dimensional velocity field is to be equally spaced so that the DFT-IDFT technique of taking partial derivatives of the translational velocities is used. A program was written in C along with MATLAB® which performed the theoretical calculations.

Two proposed methods of experimentally verifying the angular velocity data is developed using a Kistler translational/angular piezobeam accelerometer to compare against the DFT-IDFT partial derivative technique for calculating the angular velocities.

Dedication

Robert Lee DeVlaminck
(27-March-1963 to 18-July-2001)

Acknowledgements

I would like to thank the members of my graduate committee, Professors Larry D. Mitchell, Robert L. West, Alfred L. Wicks, and Donald J. Leo. Each contributed in some way to my understanding and development of my research work and as an engineer. Dr. West's insight into the Zonic project helped me understand how every piece of the puzzle was to fit. Dr. Wicks helped to motivate me with his high expectations. Dr. Leo generously gave of his time to review and make recommendations to improve this thesis. Most of all, I deeply appreciate the patience, knowledge, and understanding that Dr Mitchell gave me, and which helped me complete the work shown in this thesis. Not many such highly ranked professors, who are very involved in many other activities, would take the much appreciated time out of their busy schedule to meet with their students on a regular basis.

I would like to thank my fellow employees and management staff for encouragement, advice and for affording me the opportunity to complete this thesis.

I would like to thank Zonic Corporation for the financial support which made this research possible.

Finally, I would like to thank my wife for all the love, support and understanding that she gave me throughout my Master's studies.

Table of Contents

List of Illustrations

List of Tables

Nomenclature

Mathematical Symbols or Function

∇	"Del" operator $= \frac{\partial}{\partial x}\boldsymbol{i} + \frac{\partial}{\partial y}\boldsymbol{j} + \frac{\partial}{\partial z}\boldsymbol{k}$
Curl()	Curl function of an argument $= \nabla \times ()$
Re	Real
Im	Imaginary

Roman Letters

A	Area
A_{mn}	Amplitude constant of the m and n mode
a,b	Length of side of a rectangular plate in the x and y directions
C	Constant
C	Piecewise smooth closed curve
D	Fixed axis
D_x, D_y	Displacement field in the x, and y directions
d_1,d_2,d_3	Physical distance measurements
E	Modulus of Elasticity
$\boldsymbol{F}()$	Any differentiable vector function
F_x,F_y,F_z	Components of a differentiable vector function in the x, y and z axis directions
f	Frequency
f_{mn}	Natural frequency for the m and n mode
f_N	Nyquist frequency
f_n	Natural frequency
f_s	Sample frequency

h	Plate thickness
$\boldsymbol{i}$	Unit vector along the x-axis
$\boldsymbol{j}$	Unit vector along the y-axis
$\boldsymbol{k}$	Unit vector along the z-axis
L_x, L_y	Length along x and y directions
$_{\mathrm{m}}$	Measured variable
m,n	Mode indices in the x and y directions
N	Number of data points
N_i	Shape functions with i representing the different nodes
$\boldsymbol{n}$	Unit vector in the normal direction about a surface
P	Center of a circular disk
$\boldsymbol{R}$	Radial position vector
$\boldsymbol{r}$	Unit vector along the r-axis
S	Surface
u	Displacement along the x-axis
$\boldsymbol{V}$	Velocity vector
V_t	Tangental velocity
V_x,V_y,V_z	Components of translational velocities in x, y and z axes directions
v	Displacement along the y-axis
W_{mn}	Mode shape of the m and n mode
$\dot{W}$, $\frac{dW}{dt}$	Velocity mode shape
w	Displacement along the z-axis
x,y,z	Displacement along respective axis
$\dot{x}, \dot{y}, \dot{z}$	Velocity along respective axis
$\ddot{x}, \ddot{y}, \ddot{z}$	Acceleration along respective axis

Greek Letters

Δ	"Delta" – a change or difference between two states (points), spatial resolution
$\Delta x, \Delta y$	Spacing of spatial data points
$\boldsymbol{\phi}$	Unit vector along the ϕ-axis
$\boldsymbol{\theta}$	Unit vector along the θ-axis
$\theta_x, \theta_y, \theta_z$	Angular Displacement about the *x*, *y* and *z* axes
$\dot{\theta}_x, \dot{\theta}_y, \dot{\theta}_z$	Angular velocity about the *x*, *y* and *z* axes
$\ddot{\theta}_x, \ddot{\theta}_y, \ddot{\theta}_z$	Angular acceleration about the *x*, *y* and *z* axes
ρ	Mass density
ν	Poisson's ratio
ω	Angular velocity
ω_f	Angular forcing frequency
Ω	Angular velocity amplitude
$\Omega_x, \Omega_y, \Omega_z$	Angular velocity amplitude about the *x*, *y*, and *z* axes
ξ, η, ζ	Parametric coordinate system

Chapter 1

Introduction

The research presented in this thesis is part of a larger research project in the Structural Imaging and Modal Analysis Laboratory at the Mechanical Engineering Department of Virginia Polytechnic Institute and State University (Virginia Tech). This thesis discusses a theoretical development of the extraction of structural angular velocities. The method is then tested analytically to show its effectiveness and shortcomings.

Today, traditional experimental modal analysis is usually performed with translational accelerometers and a force transducer. The accelerometer in most cases only measures the outward normal to the structure, ignoring the in-plane motion. Assuming that a hundred points of data needed to be gathered on the surface of a structure, measuring a hundred points individually would take quite some time. Some laboratories might have the capability to measure a hundred points simultaneously with multi-channel data acquisition systems. That's great but to buy a hundred accelerometers and a hundred signal conditioners is expensive, complex to operate, lack reliability and are time consuming to calibrate. Adding them to a structure will change the mass and, therefore, the dynamics. If one wishes to measure accelerations in the x, y and z directions, one would have make a hundred measurements with tri-axial accelerometers to obtain the in-plane motions. This totals 300 signals to be processed. This adds expense and mass to the problem. Until more recently, most investigators have just been accepting the faults and limitations in the measurement and not looking for other possible methods to perform modal analysis more proficiently and completely.

Research at Virginia Tech has been geared towards improving this method of data acquisition in modal analysis. Instead of using an accelerometer, the device being used is

the Laser Doppler Vibrometer (LDV). The LDV measures the velocity of the structure along the line-of-sight of the laser beam. The goal of the group research project is to implement the results of the LDV measurements into a piece of software to calculate the six degrees-of-freedom (three translational and three rotational) of an array of points on the structure.

1.1. Overview of the Six Degree-of-Freedom Project

The research and development of the methods used in the program to obtain the six degrees-of-freedom were distributed into the following different categories:

- Shape Model
- Data Acquisition
- Registration
- Functionalization
- 3-D Reconstruction
- Angular Velocity Extraction
- 3-D Spatial Visualization

These categories are presented in a process-flow diagram in Fig. 1-1. In the following text the categories will be explained and references given for further details.

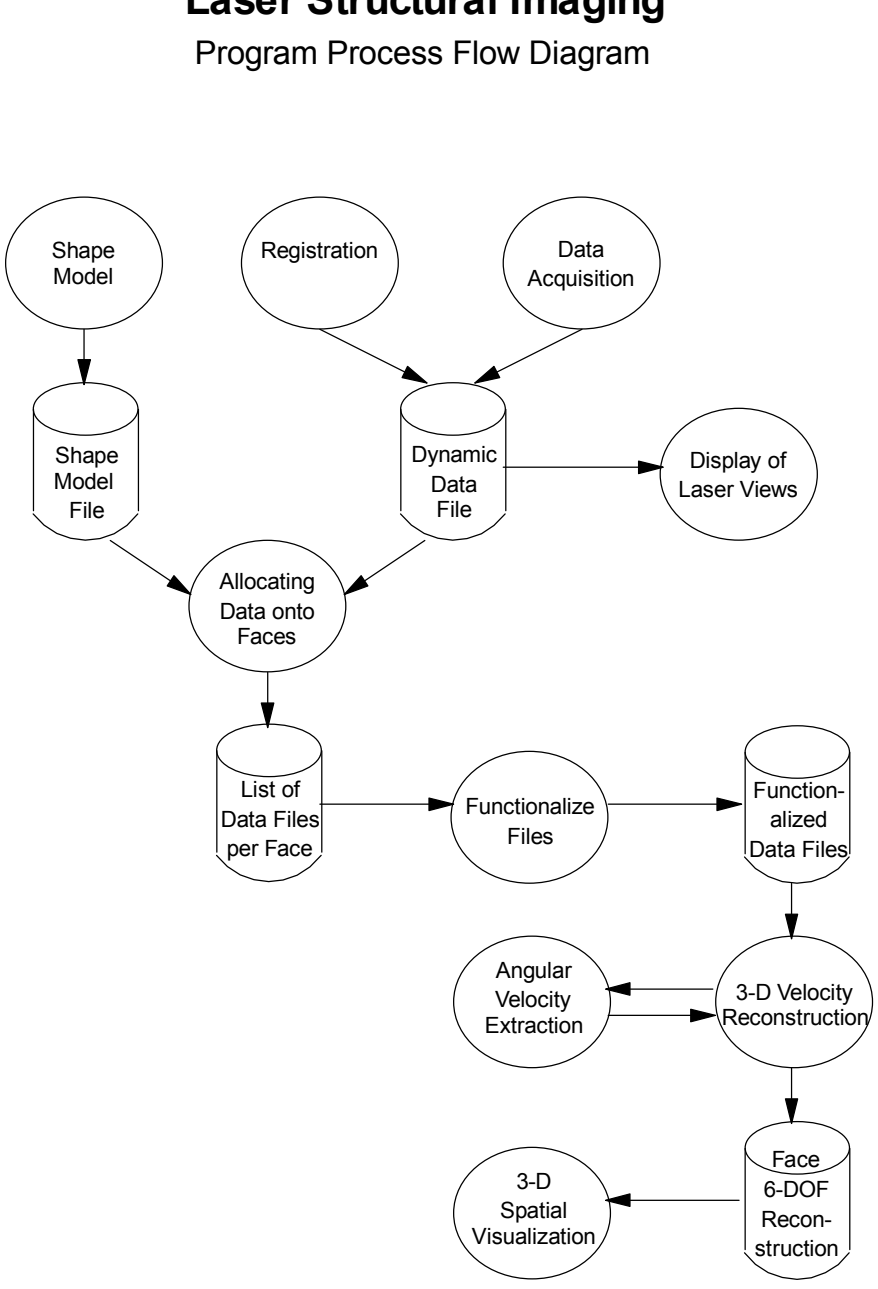

Figure 1-1: Laser Structural Imaging Program Process Flow Diagram

The shape model gives us a framework into which we reconstruct our dynamic data. The shape model contains the global coordinate system. The geometric shape of the object must be known so that all collected laser data can be related to an x, y and z location. For our study the shape model consists of polygonal elements who share common vertices.

Every time the laser is positioned in front of a structure to be scanned, it must be registered. In other words, the laser position with respect to the structure to be scanned must be known. This is done by knowing four or more points of the structures global coordinates and by aiming the laser at these points while recording the laser aiming parameters. A transformation matrix is then calculated relating the structure's global coordinate system to the laser's coordinate system. The registration process and its used in this project is reported by Zeng in [1,2,3].

Data can be obtained with the LDV through various ways. One way is to position the laser beam to a predetermined set of points. The laser beam is positioned with two galvanometrically driven mirrors from within the laser housing. The mirrors move the laser beam up, down, left and right relative to the laser coordinate system. To position the laser at a select number of points, the angular positioning of the mirrors must be calculated. Computationally, this is very time consuming for a person taking data out in the field. It is desired to spend computational time in data analysis, not in data acquisition. Thus, it is chosen to take data at equal mirror angle increments. When taking data with this method, it is necessary to functionalize the data to later reconstruct the velocities at any selected location. There are many methods for the functionalization process. For this project, the Discrete Fourier Transform (DFT) was used to reach the goal. Since the DFT is related to the Fourier Series and it is known that the Fourier Series can describe any periodic function; in theory the DFT should be able to perform well if the data is periodic I the spatial window. The Discrete Fourier Transform can describe any discrete, periodic function as long as the sampling criterion is met. Specifics as to how this functionalization routine is implemented is reported by Neumann's Thesis

[4] and a paper by Neumann [5]. The data acquisition is described by Lopez Dominguez [6].

The next step is to reconstruct the three-dimensional velocity field. First, there must be a minimum of three different non-coplanar laser viewing positions used for the collection of data upon each structural face. For every point upon the face, the laser velocity vector data should span a three-dimensional space. In other words, the laser should be placed in well-separated vantage points so as not to be coplanar. The structure is subdivided into faces and each face is logically subdivided at corners and edges unless the object is spherical. If the object is spherical then one would divide the sphere into sections. Three laser scans can be made in each section. This may be able to be obtained by dividing the sphere into six parts as if one put an imaginary box around it. For each laser scan (or data set) the data is run through the functionalization process. The faces are then meshed with a desired grid evenly spaced in a parametric coordinate space. (These grid points are then element vertices in the dynamic model.) Then these points are reconstructed by first evaluating the functions of each laser scan for the particular point in the parametric space. With a minimum of three laser vectors that span a three-dimensional space, these vectors are then transformed into an orthogonal triad of velocity vectors aligned in the directions of the global coordinates. The details of how the reconstruction and transformation of the velocity vectors are performed are reported by Neumann and Abel, respectively [4,8] as well as others [9].

The first three degrees-of-freedom of information for the selected points is what has been obtained so far. It is desired to have the rotational velocities as well. This is where the research in this thesis comes into play. The next step is to take the three-dimensional velocity information that is evenly spaced in the parametric coordinate for use in the extraction of the angular velocity information. This can be done several ways, but the DFT-IDFT approach is used once again as was to functionalize the initial velocity scans by Neumann [4]. Spatial derivatives of this data are taken in the spatial frequency domain. This process will be explained within this thesis.

Finally, all of the six degrees-of-freedom information are mapped to the shape model to form the dynamic model. This model is then animated so that the user can visually see what is dynamically occurring in the structure. For details as to how this visualization process takes place, the reader is referred to the work of Montgomery [10,11].

1.2. The Rotational Degrees-of-Freedom Portion of Project

The rotational degrees-of-freedom portion of the project will be reviewed within this thesis. There are various methods by which one can extract the angular velocities. Chapter 2 of this thesis will review the literature on how others have handled this problem.

Chapter 3 will explain why the DFT-IDFT method was chosen and how it is used for angular velocity extraction. The theoretical development of the curl function will be shown mathematically. Then the curl is applied to a two dimentional beam to show how it results in the same equation that is learn in a beginning mechanics of materials course. Assumptions will be listed concerning the practical use of this method.

Chapter 4 will demonstrate the use of the DFT-IDFT method using analytical equations. The results of the DFT-IDFT method will be compared to the exact solution of the analytical partial derivatives.

Chapter 5 will develop or explain a proposed experimental procedure to compare the results of the angular velocity extraction routine with that of an experiment using three Translational-Angular PiezoBEAM® (TAP®) System of Kistler accelerometers or equivalent rotational-translational accelerometer system.

Chapter 6 will draw conclusions based upon this work and give recommendations for future work in this area.

Chapter 2

Literature Review

This chapter is a review of existing literature on experimentally extracting the rotational degrees-of-freedom information of a vibrating structure. The history of experimentally determining the rotational degrees-of-freedom will be explored in order to justify its significance. The most recent and concurrent research that is occurring both here at Virginia Tech and abroad will also be discussed.

2.1. Establishing the Need for Rotational Degree-Of-Freedom Information

Mitchell [12] stated the need for adding the rotational degrees-of-freedom to the modal vectors of experimental modal analysis (EMA) so that it can be compared to the results of finite element analysis (FEA). Typically, FEA packages contain usually two sometimes three angular degrees-of-freedom as well as three translational degrees-of-freedom at each node. Until recently, EMA only measured the translational degrees-of-freedom. By having these added rotational degrees-of-freedoms, structural dynamics modification will better match results of FEA as well as what happens to the actual structure [13, 14].

Through Mitchell's presentation [12] of this much needed addition to EMA, there has been an accelerometer capable of measuring one rotation as well as one translation developed by Kistler Corporation. As stated in Chapter 1, the addition of an accelerometer to a lightweight structure can change the dynamics of such a structure. If three of these accelerometers were mounted in a tri-axial manner on a lightweight structure, even more of a mass and mass moment loading problem could be seen. Moreover, each structural point will require the processing of six signals. A 100 structural point measurement will require the processing of 600 signals. There is also the problem of coupling between the angular accelerations and the translational accelerations.

This occurs when the three accelerometers are mounted onto a block, which puts the accelerometers farther away from the neutral axis of the structure. Therefore, the need arises for a non-intrusive method of obtaining the three rotational and three translational degrees-of-freedom. A non-intrusive method to obtain these six degrees-of-freedom is partially presented within the research of this thesis.

As can be seen, there is a great need for obtaining the rotational degrees-of-freedom as well as a non-intrusive method to obtain the motion of a vibrating structure. In [15] there are several methods discussed for non-intrusive methods of obtaining response data as well as non-intrusive excitation techniques.

2.2. Early Attempts to Measure the Rotational Velocities

Researchers in the earlier days knew that in order to verify their analytical results they must obtain all six degrees-of-freedom of information to fill the mobility matrix. These researchers developed many methods for measuring the rotational terms in the mobility matrix.

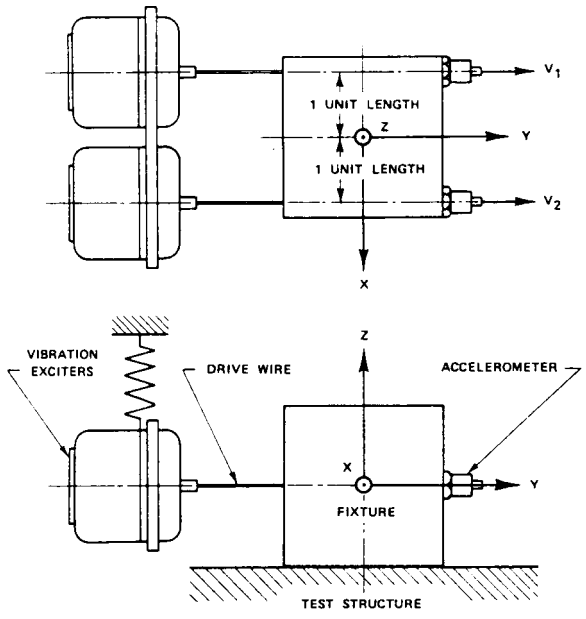

Figure 2-1: An exciter block as developed by Smith (After ANSI S2.34-1984 [18])

Smith [16] introduced the concept of attaching a vibration exciter to a structure of interest. With the aid of this excitation fixture, the full dynamic response data can be collected to complete the total structural mobility matrix. Figure 2-1 shows one example of such a vibration exciter. Two shakers are attached to a solid cube that allows both forces and moments to be applied to the structure. These forces and moments are not measured with force transducers but with the aid of two accelerometers. These accelerometer

measurements are proportional to the unknown elements of the structural mobility matrix. In [16] there are other designs and shapes for vibration exciters. Examples are cubes with voids, cylinders and cylinders with voids.

Ewins and Sainsbury [17] shortly after Smith [16] developed their version of a vibration exciter. They reduced the 6 x 6 total structural mobility matrix to their desired 3 x 3 structural mobility matrix. Figure 2-2 and 2-3 shows their two attempts at designing such fixtures. These fixtures would incorporate the use of a single shaker that can be placed in different positions to obtain three excitation directions (F_x, F_y and M_θ). After completing the design of MK 1 and analyzing the equations, it was found that errors of 0.01% in amplitude and 0.01° in phase would generate large errors (>5dB) in computed mobilities. Following the results of MK 1, MK 2 was developed. Errors of 1% in amplitude and 1° in phase, in the MK 2 design, resulted in errors of less that 1 dB in the computed mobility matrix, which is far more acceptable.

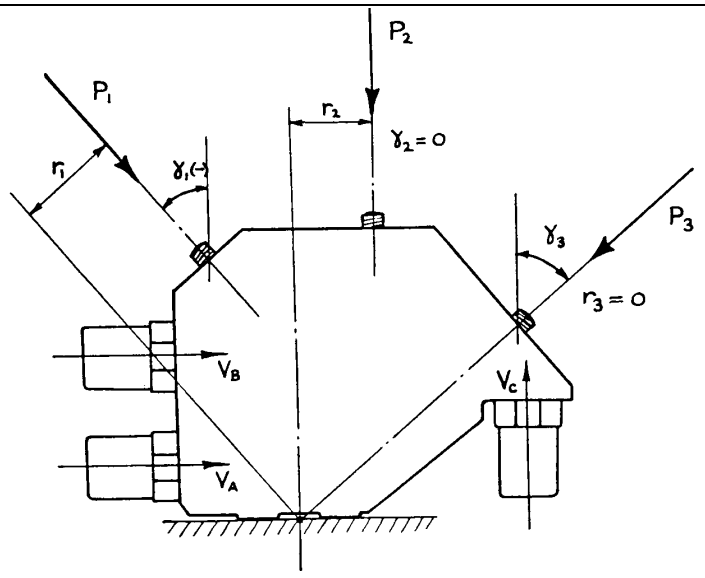

Figure 2-2: Exciting block MK 1 (not to scale) (After Ewins et al. [17])

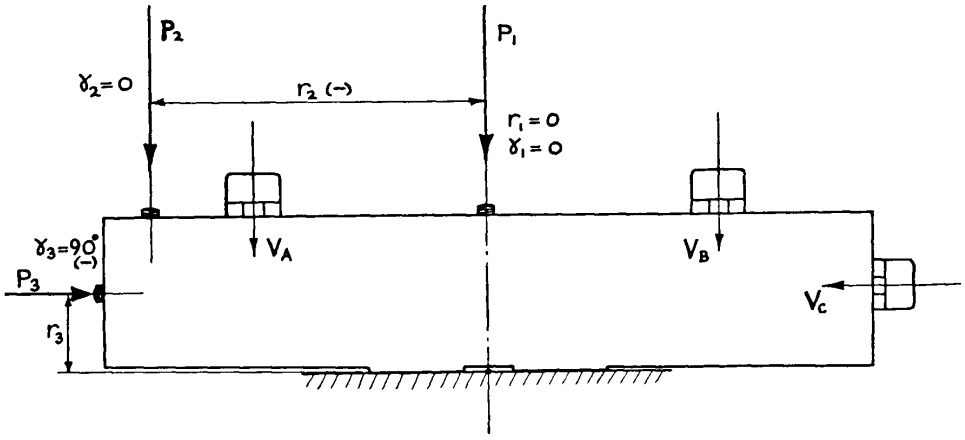

Figure 2-3: Exciting block MK 2 (not to scale) (After Ewins et al. [17])

The American National Standards Institute (ANSI) issued a Guide [18] in experimentally obtaining the rotational mobility properties to complete the total structural mobility matrix. The research of Ewins and Sainsbury [17] as well as Smith [16] was included within this Guide. A Guide was issued rather than a Standard because the state in which the art of experimentally obtaining rotational motion and rotational forces was unstable at the time of issue.

Morris et al. [19] has developed a tri-axial angular vibration measurement system. This device as shown in Fig. 2-4 is filled with a fluid substance. A vane is placed with-in this fluid that is free to rotate about its cylindrical axis which contains a sensor unit that when displaced produces a signal equal to the torque. By knowing the moment of inertia and the torque the angular acceleration can be backed out. The initial purpose of their research was to use the design on aircrafts to collect vibration data. This design has specifications that state the spectrum frequency range as being from 1 Hz to 2000 Hz.

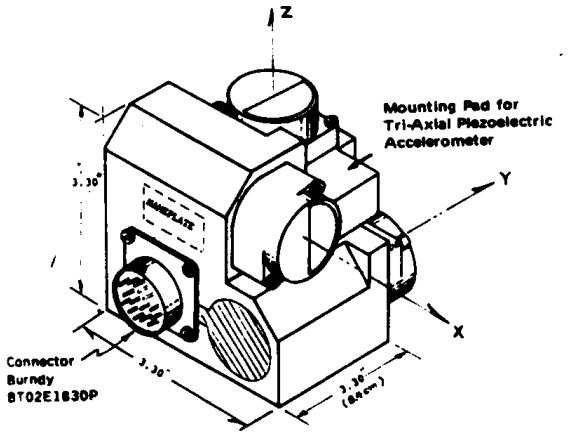

Figure 2-4: The 5690 Tri-Axis as developed by Systron-Donner Corp. (After Morris et al. [19])

Yet another method, a mass additive technique for estimating the rotational degrees-of-freedom was employed by Yasuda et al. [20]. The measurement fixture is shown in Fig. 2-5. They measure the frequency response functions (FRFs) of the structure using random excitation then estimate the rotative FRFs using a least squared error technique. Next, the modal parameters are estimated using a complex exponential fit. Finally, a mass modification procedure is implemented to compensate for the added mass to the structure. There is still more work to be performed in this area of additive mass technique in order to rid itself of errors when used with structures more complex than simple beams.

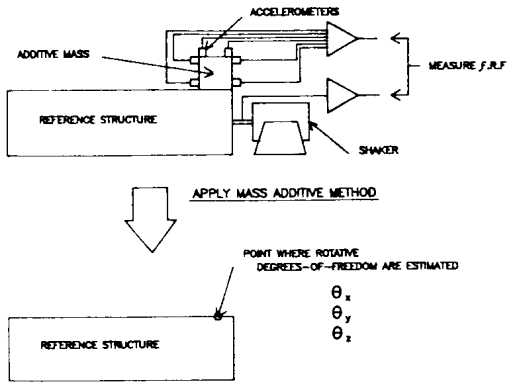

Figure 2-5: Procedure for mass additive technique (After Yasuda et al. [20])

2.3. Recent Research of Rotational Degrees-of-Freedom Measurements

Lasers have been used for quite some time in the area of fluid flow. As described in [Ptacnik et al. 21], small particles are mixed into a fluid and the velocity of the particles is measured by the laser. The assumption is the particle velocity represents that of the surrounding fluid velocity. In [Ptacnik et al. 21] the researchers were trying to define the velocity flow pattern inside and close to a rotating pitched blade impeller. This is just an example of the use of lasers in an area of fluid dynamics.

Recently lasers have been used to measure the translational vibrations of structures, and even more recently the rotational vibrations of structures. In Taubner and Martens [22] a technique was developed to measure angular acceleration, angular velocity and angular displacement with the use of diffraction grating interferometers. The experiment was done using two different types of diffraction grating interferometers; a holographically manufactured sine-phase grating on the lateral surface of a circular disk and a lithographically manufactured radial grating on the top surface of a circular disk.

Although this method of measuring rotations is good for things such as shafts, there is more of an interest in the total six degree-of-freedom dynamic response of a non-rotating structure.

In Lewin et al. [23] another technique is presented to measure the rotational motion of a rotating body. This technique does not include the addition of a diffraction grating disk being place upon the structure. This technique measures the components of the tangential velocity that can be seen from the laser line-of-sight with two laser beams measuring at two locations of a rotating shaft or disk. The two laser beams are parallel to each other and their distance apart is known which allows for a simple calculation of the rotational velocity and its direction, assuming the diameter of the shaft or disk is known. This methodology conforms to our non-intrusive measurement philosophy, but still only gives a fraction of the information desired.

Research at Imperial College in London is being done to develop a system to measure a structure's translational and angular vibration using a laser Doppler vibrometer. The technique as described by Stanbridge et al. [24] is to measure two angular vibrations along the in-plane axis's and one out-of-plane translation of the point on the structure. Circular scanning about a point to obtain these three variables does this. The angular vibrations are extracted from the frequency response function of the LDV signal divided by a reference signal. The reference signal consists of the input force signal multiplied by the mirror drive signals. The researchers tested the method with both a sine excitation and a narrow band random excitation. The advantage of this method is it attempts to incorporate more than just a single frequency. Disadvantages of this method are that it lacks the other three degrees-of-freedom needed for a complete representation of the modal vectors to compare with FEM and for use with structural dynamics modification. It is a point to point method, which would require excessive scanning times.

Researchers at Pennsylvania State University (Penn State) developed a method to measure one translation and two rotations [25,26,27]. Figure 2-6 shows the particular set-up of the laser system for such a measurement. The figure shows the use of two lasers along with two separate two-dimensional photodetectors that measure the laser beam reflections of their corresponding lasers from the target mirror. A planer mirror attached to the vibrating surface reflects the laser light source. The system measures the vertical translation (z), roll (x) and pitch (y) angular deflections of a planar target. The photodetectors output voltage signals are proportional to the time varying x-y coordinates of the reflected laser beam onto the photodetectors. The Penn State researchers used a kinematics closure principle developed in [Ulcker et al. 28] to extract the three unknown variables from the known x-y locations of the laser beam on the two photodetectors. The variables were extracted by two methods: iterative least squares and explicit solutions. The iterative least squares was chosen over the explicit solution because even though it is slower the results were more accurate.

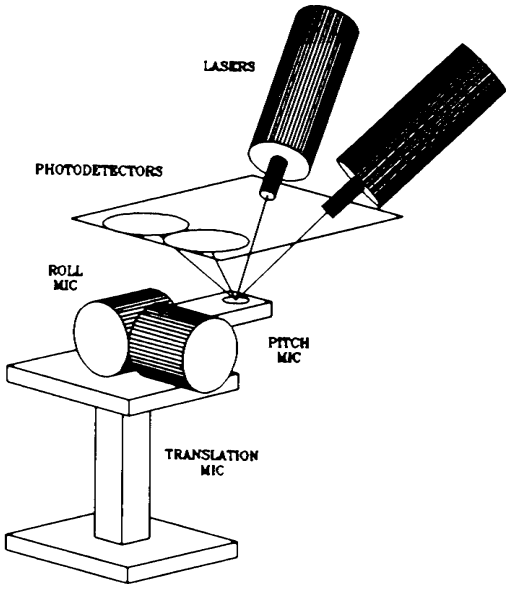

Figure 2-6: Pennsylvania State University's dual laser beam set-up (Adapted from Trethewey et al. [25])

This method of extracting the three variables using two lasers and two photodetectors was later reduced to one laser and two photodetectors [Sommer et al. 29]. Figure 2-7 shows the single beam laser vibrometer set-up developed by Penn State. In this set-up the photodetectors are transparent so the beam passes through the first in order to register any signal onto the second photodetector. The advantage of this system over the dual-laser beam set-up is less hardware and smaller overall size. The single laser beam set-up incorporates an iterative least squares solution that is used in the dual-laser beam set-up as well.

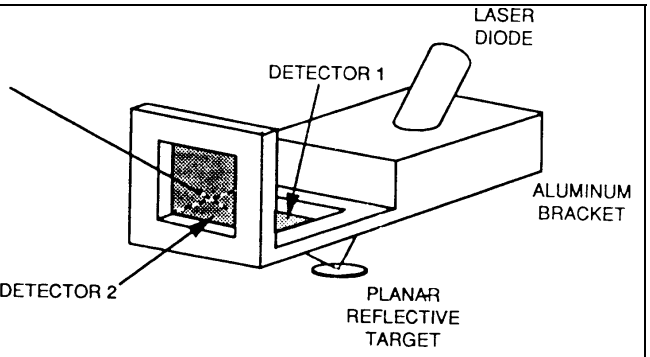

Figure 2-7: Pennsylvania State University's single laser beam system set-up (After Sommer et al. [29])

Penn State researchers also developed a laser system to simultaneously measure the six degrees-of-freedom of a point located on a structure [Bokelberg et al. 30]. Figure 2-8 easily shows the conceptual design for this six degree-of-freedom vibration measurement system. Penn State incorporates the use of three lasers and three photodetectors. The laser beams are reflected using a tetrahedral target with mirrored facets placed on the surface of a vibrating structure. The six degrees-of-freedom are calculated using the x-y voltages from the three photodetectors. In Bokelberg et al. [30] the theoretical development for calculating the six variables was not presented, but it had referenced other

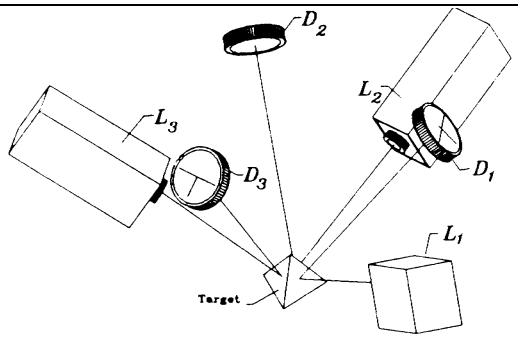

Figure 2-8: Pennsylvania State University's six degree-of-freedom vibration measurement system (After Bokelberg et al. [30])

papers which were in review for a technical paper publication. Therefore, further information on this method is not available at the time of writing this thesis.

The disadvantage of the methods used by the researchers from Penn State is the laser system set-up must be moved to each of the desired locations for measurement when gathering a vast number of data points. This is very time consuming. An advantage of the Penn State system is that it measures the rotational degrees-of-freedom directly from the structure instead of fitting functions through translational data and taking derivatives of them in order to obtain the rotational data information. In Cafeo et al.[26] an argument is made that through taking the derivative of a function that fits through a noisy translational data set can produce large errors.

Kistler Instrument Corporation has developed a transducer that measures both translational and angular accelerations, which they refer to as 8832A Translational-Angular PiezoBEAM® (TAP®) system. If this were arranged in a tri-axial fashion it would prove to be more useful in obtaining the full six degree of freedom data. The problems are dealing with the off-axis measurements in the individual directions. A method to verify this thesis's proposal for computing angular velocity in Chapter 5 uses this transducer. The equations are developed to correct for off-axis errors. If this technique were solely used, one would need many data points, which would add more data acquisition time and add weight to the structure

2.4. A Brief Discussion of Data Functionalization and Derivatives

There has been some work performed with taking the translational data across the face of a structure and fitting a function across it. For example, Ng'andu et al. [31] presents their work on estimating the rotational degrees-of-freedom by the use of curve and surface fitting. Ng'andu discusses the use of B-spline curves and bicubic surfaces as the basis functions used to extract the rotational degrees-of-freedom. Using this method allows for unequally spaced data. In Ng'andu et al. [31] there is no mention of handling plates or shells structures with holes, but if changes are made then it may be possible to

handle holes in structures. Ng'andu also presented the knowledge for the need of rotational degrees-of-freedom for structural dynamics modifications.

There are so many function types in which to fit through data over a surface and they all have their advantages and disadvantages. All possible functions available must be evaluated in order make an informed decision. In this research, the DFT-IDFT method of functionalization is used. The DFT procedure, in theory, fits any set of data as long as the Nyquist sampling theorem is followed. However, the resulting Fourier transform may have significant leakage if the original spatial data is not periodic in the time window. This is why periodization [32] is necessary to control this phenomenon.

The research presented in this thesis follows after some of the work presented by Galaitsis [33]. Prior to Galaitsis, Kochersberger [32] developed a method for angular velocity extraction using a DFT-IDFT technique. This technique calculates the angular velocities about the in-plane axes. Sun [34] extended Kochersberger's [32] work by analyzing how to filter out the noise that dramatically effects the derivative process. Galaitsis uses the DFT-IDFT angular velocity extraction technique and applies it to the in-plane velocities to obtain the "drilling modes" (or the angular velocities about the out-of-plane axis). This thesis will extend beyond what these researchers have done and also incorporate some experimental data.

Arruda [35] gives yet another method of surface smoothing. His work estimates regressively the coefficients of a two-dimensional Discrete Fourier Series with arbitrary period and frequency. This is essentially a Regressive Fourier Transform. This method can be used with non-equally spaced and non-rectangular data and minimizes leakage, since the regressive approach does no demand periodicity of the data. Partial derivatives of this function can be made in order to obtain the in-plane angular velocities. This method can be extended to take care of holes in a structure's face, but with a great computational cost as discussed with Mitchell [36].

In summary, there are very few methods that measure the full six degrees of freedom. Those that actually measure all six degrees of freedom, measure at only one point.

Mapping a whole surface with this method would be very labor intensive, not to mention any drift in the structures modes due to temperature.

Chapter 3

Theory

This chapter summarizes the theoretical development of the equations used to obtain the rotational degrees of freedom presented in this thesis study. First the curl function is defined and then its role in the study of rotational degrees of freedom is explained with some examples from mechanics of materials to show its validity. The DFT-IDFT method of taking partial derivatives is explained and shown which is necessary in evaluating the curl function. Finally, assumptions in using the resulting final equation are then summarized at the end of the chapter.

3.1. The Curl

You might ask yourself, "what is the curl function?" Webster [37] defines the word curl as "anything with a curled shape". The mathematical description of the curl function explained here can be found in many vector calculus textbooks [38]. To begin, let

$$\boldsymbol{F}(x,y,z) = F_x\boldsymbol{i} + F_y\boldsymbol{j} + F_z\boldsymbol{k} \tag{3.1}$$

be a differentiable vector function and x, y, z be the right-handed Cartesian coordinate system in space. Kreysig [38] defines the curl of a vector function $\boldsymbol{F}$ as

$$curl\ \boldsymbol{F} = \left(\frac{\partial F_z}{\partial y} - \frac{\partial F_y}{\partial z}\right)\boldsymbol{i} + \left(\frac{\partial F_x}{\partial z} - \frac{\partial F_z}{\partial x}\right)\boldsymbol{j} + \left(\frac{\partial F_y}{\partial x} - \frac{\partial F_x}{\partial y}\right)\boldsymbol{k} \tag{3.2}$$

Another, representation that Kreysig [38] as well as many other vector calculus books like Ellis et. al. [39] define the curl as

$$curl(\boldsymbol{F}) = \nabla \times \boldsymbol{F} \tag{3.3}$$

where ∇ ("Del") is defined as

$$\nabla = \frac{\partial}{\partial x}\boldsymbol{i} + \frac{\partial}{\partial y}\boldsymbol{j} + \frac{\partial}{\partial z}\boldsymbol{k} \tag{3.4}$$

in the Cartesian coordinate system. Another expression offered by Kreysig that is easy to remember is

$$curl(\boldsymbol{F}) = \begin{vmatrix} \boldsymbol{i} & \boldsymbol{j} & \boldsymbol{k} \\ \dfrac{\partial}{\partial x} & \dfrac{\partial}{\partial y} & \dfrac{\partial}{\partial z} \\ F_x & F_y & F_z \end{vmatrix} \tag{3.5}$$

that when this determinant is expanded it is equivalent to Eq. (3.2). Let it also be noted that sometimes the notation rot $\boldsymbol{F}$ (rotation of $\boldsymbol{F}$) is sometimes used instead of curl $\boldsymbol{F}$ in some text.

The equations previously shown for the curl of a vector field were all in the Cartesian coordinate system. Sometimes cylindrical or spherical coordinate systems are more convenient to use than the Cartesian coordinate system. The curl of a vector field for the cylindrical coordinate system is:

$$curl(\boldsymbol{F}) = \left(\frac{1}{r}\frac{\partial F_z}{\partial \theta} - \frac{\partial F_\theta}{\partial z} \right)\boldsymbol{r} + \left(\frac{\partial F_r}{\partial z} - \frac{\partial F_z}{\partial r} \right)\boldsymbol{\theta} + \left(\frac{1}{r}\frac{\partial (rF_\theta)}{\partial r} - \frac{1}{r}\frac{\partial F_r}{\partial \theta} \right)\boldsymbol{z} \tag{3.6}$$

In spherical coordinates the curl is given as

$$\begin{aligned} curl(\boldsymbol{F}) = &\left(\frac{1}{r\sin\theta}\frac{\partial \sin\theta\, F_\phi}{\partial \theta} - \frac{1}{r\sin\theta}\frac{\partial F_\theta}{\partial \phi} \right)\boldsymbol{r} + \left(\frac{1}{r\sin\theta}\frac{\partial F_r}{\partial \phi} - \frac{1}{r}\frac{\partial (rF_\phi)}{\partial r} \right)\boldsymbol{\theta} \\ &+ \left(\frac{1}{r}\frac{\partial (rF_\theta)}{\partial r} - \frac{1}{r}\frac{\partial F_r}{\partial \theta} \right)\boldsymbol{\phi} \end{aligned} \tag{3.7}$$

3.1.1. Mathematical Examples and Physical Interpretation of the Curl

Previous to this section the curl function was shown but not developed. Many engineers are familiar with at least the name of the theorem, Stokes's theorem. Stokes's theorem allows for a transformation of surface integrals into line integrals and the inverse. The Stokes's theorem begins with a piecewise smooth oriented surface in space, *S*, and the boundary of *S* is a piecewise smooth closed curve *C* as shown in Fig. 3-1. The curve *C* encloses the surface area *S* with *S* always being on the left. Using the right-hand rule following the curve *C*, the normal points up. Within this surface space *S*, let $\boldsymbol{V}(x,y,z)$

be a continuous velocity vector function with continuous partial derivatives. Stokes's theorem then states the following equation.

$$\iint_S (curl\boldsymbol{V})_n \, dA = \int_C V_t \, dS \tag{3.8}$$

Where

$$(curl\boldsymbol{V})_n = (curl\boldsymbol{V}) \cdot \boldsymbol{n} \tag{3.9}$$

is the component of curl $\boldsymbol{V}$ in the direction of the unit normal vector $\boldsymbol{n}$ and V_t is the component of $\boldsymbol{V}$ in the direction tangent to the curve C. The proof of Stokes's theorem, for purposes of this study, can be found in Kreysig [38].

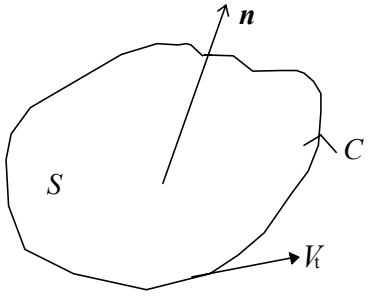

Figure 3-1: An illustration for Stokes's theorem

A physical interpretation of the curl using Stokes's theorem is also shown Kreysig [38]. The following will be a brief summary of the physical interpretation of the curl using Stokes's theorem. We will begin with Stokes's theorem shown earlier

$$\int_C V_t \, dS = \iint_S (curl\,\boldsymbol{V})_n \, dA = [curl\,\boldsymbol{V}(P)]_n \, A \tag{3.10}$$

where P is the center of the circular disk shown in Fig. 3-2 and A is the area of the surface S. If $\boldsymbol{V}$ represents the velocity of a fluid, the integral

$$\int_C V_t \, dS \tag{3.11}$$

measures the rotation of the fluid motion about the center P of the circle C. Now divide Eq. (3.10) by A, and let A approach zero, the resulting equation is

$$\left[curl\,\boldsymbol{V}(P)\right]_n = \lim_{A\to 0}\frac{1}{A}\int_C V_t dS \tag{3.12}$$

Which tells us that the curl of a vector function, $\boldsymbol{V}$, is related to the rotational motion at point P.

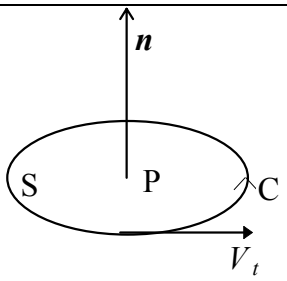

Figure 3-2: Physical interpretation of the curl using Stokes's theorem

All of these definitions are great but how is the curl related to the angular velocity field. This relationship can be shown as

$$curl\,\boldsymbol{V} = 2\boldsymbol{\omega} \tag{3.13}$$

where $\boldsymbol{V}$ is the velocity vector field and $\boldsymbol{\omega}$ is the angular velocity vector field. The reader might ask where did this equation come from, or for that matter where did all of the equations up until this point come from. Again I refer the reader to Kreysig [38] for a more thorough explanation.

A quick example of rigid-body dynamics to illustrate how we can obtain Eq. (3.13) to a rotating disk is as follows. In Fig. 3-3, we have a rigid body that rotates about a fixed

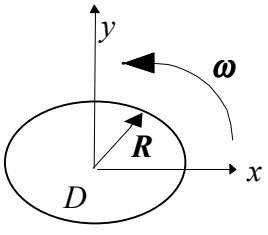

Figure 3-3: A circular disk in the *x*-*y* plane to illustrate the curl in rigid-body dynamics

axis D with a constant rotation $\boldsymbol{\omega}$ about the z-axis in a counterclockwise positive sense. Knowing that the tangential velocity is

$$\boldsymbol{V} = \boldsymbol{\omega} \times \boldsymbol{R} \tag{3.14}$$

where $\boldsymbol{R}$ is the position vector to any arbitrary point within the rotating body such that

$$\boldsymbol{R} = x\boldsymbol{i} + y\boldsymbol{j} \tag{3.15}$$

and

$$\boldsymbol{\omega} = \omega\, \boldsymbol{k} \tag{3.16}$$

When the mathematics is complete the velocity vector is as follows

$$\boldsymbol{V} = -\omega\, y\, \boldsymbol{i} + \omega\, x\, \boldsymbol{j} \tag{3.17}$$

When you apply the curl function on the velocity vector, $\boldsymbol{V}$, we arrive at

$$curl\boldsymbol{V} = \begin{vmatrix} \boldsymbol{i} & \boldsymbol{j} & \boldsymbol{k} \\ \dfrac{\partial}{\partial x} & \dfrac{\partial}{\partial y} & \dfrac{\partial}{\partial z} \\ -\omega y & \omega x & 0 \end{vmatrix} = 2\omega\boldsymbol{k} \tag{3.18}$$

which is equal to that of Eq. (3.13). Therefore, the angular velocity of a rigid body is half of the curl of the velocity vector.

3.1.2. Mechanics of Materials Examples to Validate the Curl Function

The mathematical derivations and rigid body formulation of the curl function is great, but in most real world problems we deal with deformable bodies. In deformable bodies as well as fluid bodies, the curl of the velocity vector is twice the angular velocity. Also, as an aside, the curl of a displacement vector field is also equal to twice the angular displacement.

One good example of a deformable body illustrated in Ford [40] takes a cubic element and lets it experience strains in which the its diagonal sustains a slight deformation shown in Fig. 3-4. Now look at the cube in a two-dimensional sense as in Fig. 3-5. The rotation of the element in this two-dimensional state is then defined as

$$\theta_z = \frac{1}{2}\left(\frac{dv}{dx} - \frac{du}{dy}\right) \tag{3.19}$$

where, in the 3-D state vector representing the diagonal is:

$$\boldsymbol{R} = u\boldsymbol{i} + v\boldsymbol{j} + w\boldsymbol{k} \tag{3.20}$$

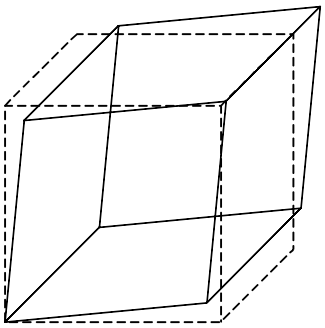

Figure 3-4: A three dimensional cubic element in shear

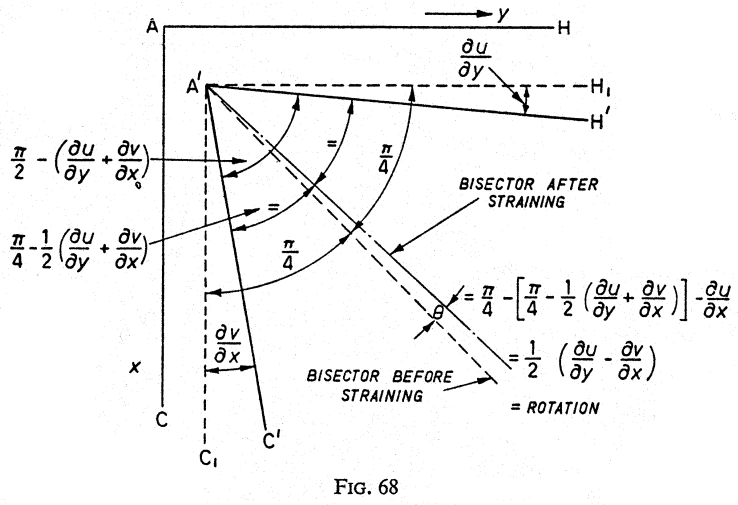

Figure 3-5: A two dimensional element in shear as taken from [40] pg. 129 Fig. 68.

The next example is used as the crutch for the work presented later in this chapter. Beam theory is generally covered in an introductory mechanics of materials course. One aspect or property covered in beam theory is the slope of the beam as it is deflected. For

a beam that experiences a deflection such as shown in Fig. 3-6, the slope as derived in

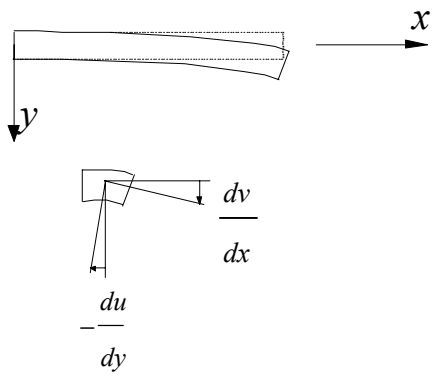

Figure 3-6: Deflection of a beam and the slope found in introductory Mechanics of Materials course.

texts such as Higdon et al. [41] to be:

$$\theta_z = \frac{dv}{dx} = -\frac{du}{dy} \tag{3.21}$$

where the displacement gradient in both directions are equal to the slope, but one is the negative of the other.. (Note, that this holds true only for small displacements

This can be applied to the curl equation where,

$$\theta_z = \frac{1}{2}\left(\frac{dv}{dx} - \frac{du}{dy}\right) \tag{3.22}$$

is the component of the curl about the z-direction. Substituting the Eq. (3.23)

$$\frac{du}{dy} = -\frac{dv}{dx} \tag{3.23}$$

into the curl function, one would arrive at:

$$\theta_z = \frac{1}{2}\left(\frac{dv}{dx} - \left(-\frac{dv}{dx}\right)\right) = \frac{dv}{dx} \tag{3.24}$$

Hence, this is the same result found in an introductory mechanics of materials course.

Equation (3.21) shows how the gradient with respect the thickness direction (y) is equal to the gradient with respect to the surface direction (x). One can take the time derivative of Eq (3.21) to obtain velocity gradients.

$$\frac{du}{dydt} = -\frac{dv}{dxdt}; \quad \frac{dV_x}{dy} = -\frac{dV_y}{dx} \tag{3.25}$$

3.2. Partial Derivatives

As the previous section shows, in order to obtain the rotational velocities of a structure the partial derivatives of the translational velocities are required. This can occur by functionalizing the translational velocity field and taking spatial derivatives of the functions or numerical difference techniques can be used. Although there are these various methods, it has been chosen for this study to use the Discrete Fourier Transform (DFT) to functionalize the data into a series of sines and cosines.

3.2.1. Why the DFT-IDFT

Sines and cosines are the functions most commonly used in the study of vibrations. They fit the theory of vibrations (oscillating motion) and the experimental measurement too. The summation of the sines and cosine terms over infinity is commonly called Fourier Series. The Fourier Series can describe any periodic function. The DFT is related to the Fourier Series and is a way to discretize an analog signal over a finite time period so as to be able to describe a periodic function. As discovered in an intermediate vibrations course the vibration of a structure in the spatial directions is generally a summation of sines and cosines terms.

In this study the velocity of a sinusoidally forced vibrating structure is being measured using the Ometron laser. Using this technology, with its rapid scanning ability, we can obtain the near continuous vibration of the surface velocity. With the high spatially dense information we can describe the total velocity field.

3.2.2. How to Carry-Out the Partial Derivatives Using the DFT-IDFT

In order to take derivatives of data using the DFT approach we must first have a periodic function. If we have a spatial function as described in Fig. 3-7(a), which is non-periodic, leakage can occur when performing the DFT. Looking at the work of Kevin

Kochersberger [42] he explains a method of shearing, mirroring and flipping non-periodic data before performing the DFT.

The first step is to shear the data so that the endpoints lie on the x-axis. Drawing a line from the first point to the last point performs this. Then subtracting out the distance of the sloped line from the zero axis from the original waveform data. This is shown in Fig. 3-7(b). Next, the data is to be mirrored and flipped, obtaining a resulting waveform twice the size of the original data. This is shown in Fig. 3-7(c). The original slope has to be recorded for later use when trying to reconstruct the data.

One may think, why not use a typical windowing function (i.e. Hanning) to make the endpoints diminish to zero, instead of shearing the data. The problem lies in reconstructing the original signal. To reconstruct the original signal, the IDFT would have to be multiplied by the inverse of the weighting function. At zero points of the time-domain weighting function the inverse would be infinity, therefore, the original equation can not be numerically reconstructed.

The general equation for the DFT is shown as:

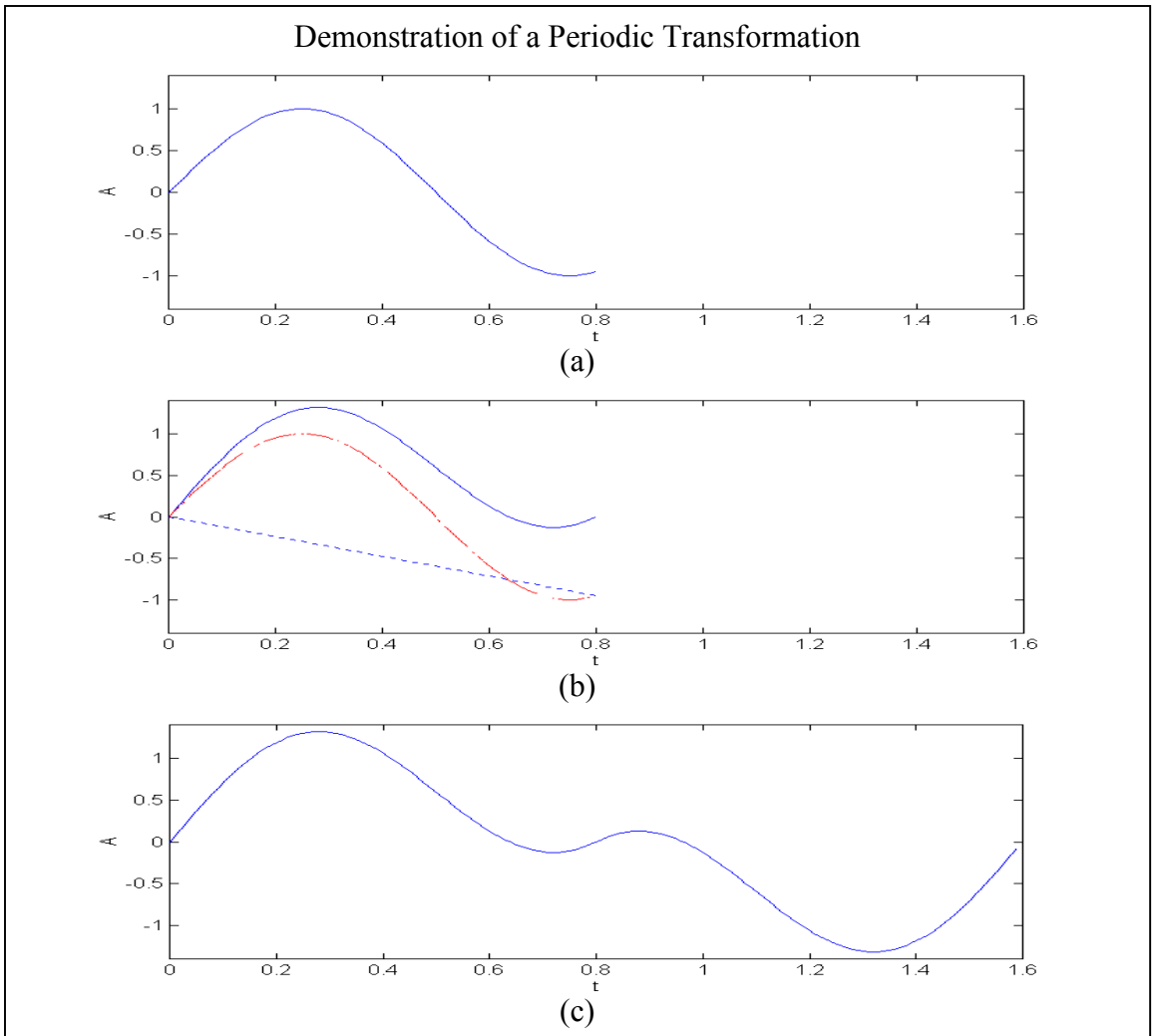

Figure 3-7: The figures above demonstrate the way to make a non-periodic data set periodic so that a DFT can be performed. The original signal (a) is a partial sign wave. (b) The sine wave is sheared to make both end points zero. (c) The resultant is mirrored and flipped to complete the periodic transformation.

$$V_y(f) = \frac{2}{N\Delta x}\sum_{x=0}^{N-1} V_y(x) e^{\frac{i2\pi fx}{N\Delta x}}; \quad f = 0,1,\ldots\frac{N}{2} \tag{3.26}$$

And using the above equation with its' notation the IDFT can be written as:

$$V_y(x) = \mathrm{Re}\left(\sum_{f=0}^{\frac{N}{2}} V_y(f) e^{\frac{i2\pi fx}{N\Delta x}} \right); \quad x = 0,1,\ldots \frac{N}{2} + 1 \tag{3.27}$$

Note that only $N/2+1$ velocities are needed since the original length of the data has been doubled. The derivatives needed to obtain the rotational velocities for the curl function can be shown as:

$$\frac{\partial V_y(x)}{\partial x} = \mathrm{Re}\left(\sum_{f=0}^{\frac{N}{2}} V_y(f) \frac{i2\pi f}{N\Delta x} e^{\frac{i2\pi fx}{N\Delta x}} \right); \quad x = 0,1,\ldots \frac{N}{2} + 1 \tag{3.28}$$

Equation (3.28) is used for the sheared, mirrored and flipped data. The slope constant must be added to get the derivative of the original equation.

3.3. How is the Curl Used on the Reconstructed Velocity?

In the previous section we developed a way to functionalize the data in order to take the partial derivatives. Now that the basic equations have been developed, we can apply it to the curl function in order to get the angular velocity field we are interested in. First let us step back and understand how the reconstructed velocity field received is obtained. In the work of Mike Neuman [4] the original laser data was functionalized in equal laser increments.

The next step is to formulate a reconstructed triad of velocity vectors [Donovan 9]. These vector triads must be functionalized per face as discussed in section 1.1 of this thesis. The faces may be irregular in shape or contain holes. In order to take the partial derivatives needed for the angular velocities, the linear velocities must be equally spaced. This is handled is by meshing the faces with rectangular or triangular parametric elements as is done in a finite element analysis.

3.3.1. Parametric Space to Geometric Space

The formulation of the transformation of the partial derivatives of the velocity field from the parametric space to the geometric space can be found in most finite element

textbooks. The following equation shows how the partial derivatives of the velocity field relates to the parametric space:

$$\begin{Bmatrix} \frac{dV}{d\xi} \\ \frac{dV}{d\eta} \\ \frac{dV}{d\zeta} \end{Bmatrix} = \begin{bmatrix} \frac{dx}{d\xi} & \frac{dy}{d\xi} & \frac{dz}{d\xi} \\ \frac{dx}{d\eta} & \frac{dy}{d\eta} & \frac{dz}{d\eta} \\ \frac{dx}{d\zeta} & \frac{dy}{d\zeta} & \frac{dz}{d\zeta} \end{bmatrix} \begin{Bmatrix} \frac{dV}{dx} \\ \frac{dV}{dy} \\ \frac{dV}{dz} \end{Bmatrix} \tag{3.29}$$

where the three by three matrix is referred as the Jacobian matrix denoted by [J]. The function V can be V_x, V_y or V_z for all three directions of the vector triad. To solve for the physical, geometric space the inverse of the Jacobian must be obtained. The equations for the x, y and z geometric space mapped to parametric coordinates can be described by the following equations for a shell element as shown in Fig. 3-8:

$$x(\xi,\eta,\zeta) = \sum_{i=1}^{N} N_i(\xi,\eta)x_i + \frac{a}{2}\zeta\sum_{i=1}^{N} N_i(\xi,\eta)n_{x_i} \tag{3.30}$$

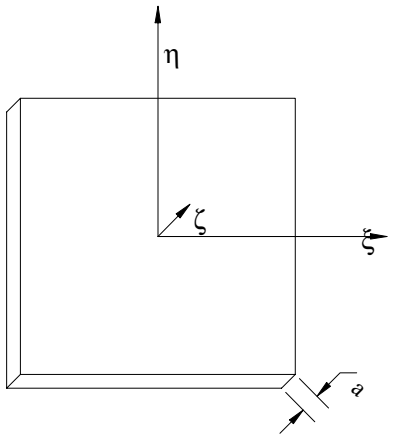

Figure 3-8: The figure above demonstrates a simple shell element in parametric coordinates.

where N is the shape functions dependent on the element shape and number of nodes. For a four node rectangular shape the shape functions are:

$$
\begin{aligned}
N_1(\xi,\eta) &= \frac{1}{2}(1+\xi)(1+\eta) \\
N_2(\xi,\eta) &= \frac{1}{2}(1-\xi)(1+\eta) \\
N_3(\xi,\eta) &= \frac{1}{2}(1-\xi)(1-\eta) \\
N_4(\xi,\eta) &= \frac{1}{2}(1+\xi)(1-\eta)
\end{aligned}
\tag{3.31}
$$

3.3.1.1. Correction for Flat Plates

The first problem we run into is taking the derivative in the ζ-direction. This requires information of velocities across the thickness of a plate or shell element. If we apply this to a flat plate we can have the *x*, *y*, and *z* coordinates line up with the ξ, *η*, and *ζ* coordinates. With this we can use the mechanics of materials example earlier, assume linear shear, and take the derivative to get velocity, which will result in the following:

$$
\begin{aligned}
&\frac{\partial V_y}{\partial z} = -\frac{\partial V_z}{\partial y}; \frac{\partial V_x}{\partial z} = -\frac{\partial V_z}{\partial x} \\
&\omega = \frac{1}{2} curl\, V = \left(\frac{\partial V_z}{\partial y}\right)\boldsymbol{i} + \left(-\frac{\partial V_z}{\partial x}\right)\boldsymbol{j} + \frac{1}{2}\left(\frac{\partial V_y}{\partial x} - \frac{\partial V_x}{\partial y}\right)\boldsymbol{k}
\end{aligned}
\tag{3.32}
$$

This will also result in the off diagonal terms of the Jacobian to be zero.

3.3.1.2. Theory for Non-Flat Plates

If the dynamic strains throughout the thickness were measured then the equations would be valid as rotational velocities are half the curl. The strains measured would be values in the parametric space and the mathematics would get ugly, but is achievable.

Chapter 4

Analytical Example

In the previous chapter, the curl function was presented. Its role in obtaining rotational velocities from translational velocities was shown. The DFT was also discussed as the method to fit the translational velocity data. Spatial partial derivatives of the DFT results were taken as a step toward obtaining the angular velocity. This chapter will use the DFT-IDFT partial-derivative technique on two analytical case studies to demonstrate the ability to obtain both in-plane and out-of-plane rotational degrees of freedom.

To fully demonstrate all six DOFs, an analytical example that has mode shapes that are both in-plane and out-of-plane motions at one common frequency would need to be utilized. It was difficult to obtain a well-documented example that includes both motions. Thus, this chapter will handle these as two separate cases: the simply supported plate and the in-plane mode with out-of-plane rotational motion (drilling degree of freedom) case.

4.1. The Simply Supported Plate

Using the simply supported plate example, the out-of-plane, analytical, vibration solutions can be found in many resources [44,45]. The in-plane translational vibrations of these structures are generally smaller in magnitude and are often at frequencies that are ten times the frequency of the out-of-plane modes. For this study the partial derivatives of out-of-plane translational motions with respect to the in-plane directions can be taken independent of the in-plane translational vibration.

The solutions to the out-of-plane modes for rectangular plates with various boundary conditions can be found in Blevins [44] and Leissa [45]. For this case study the simply supported boundary condition on all sides of a rectangular plate will be used. A model of

this thin plate configuration yields a solution for the natural frequencies and mode shapes as:

$$f_{mn} = \frac{1}{2\pi}\sqrt{\frac{Eh^2}{12\rho(1-v^2)}}\left[\left(\frac{m\pi}{a}\right)^2 + \left(\frac{n\pi}{b}\right)^2\right] \tag{4.1}$$

$$W_{mn} = A_{mn}\, sin\frac{m\pi x}{a} sin\frac{n\pi y}{b} \tag{4.2}$$

where E is the modulus of elasticity, m and n are the mode indices of x and y directions respectively, ρ is the mass density, v is Poisson's ratio, and a and b are the lengths of the sides of x and y respectively and h the plate thickness.

For this research, we are interested in obtaining translational velocities and rotational velocities. Equation (4.2) can be differentiated to obtain translational velocities. This would require a multiplication by $i2\pi f_{mn}$, leading to:

$$\dot{W}_{mn} = B_{mn}\, sin\frac{m\pi x}{a} sin\frac{n\pi y}{b}; \quad B_{mn} = i2\pi f_{mn} A_{mn} \tag{4.3}$$

Figure 4-1 shows the first four velocity mode shapes of a square plate with unit dimensions (a,b) and unit amplitude (B_{mn}). The partial derivatives of the fully simply supported velocity mode shapes can be shown to be:

$$\frac{\partial \dot{W}_{mn}}{\partial x} = \frac{m\pi}{a} B_{mn}\, cos\frac{m\pi x}{a} sin\frac{n\pi y}{b} \tag{4.4}$$

$$\frac{\partial \dot{W}_{mn}}{\partial y} = \frac{n\pi}{b} B_{mn}\, sin\frac{m\pi x}{a} cos\frac{n\pi y}{b} \tag{4.5}$$

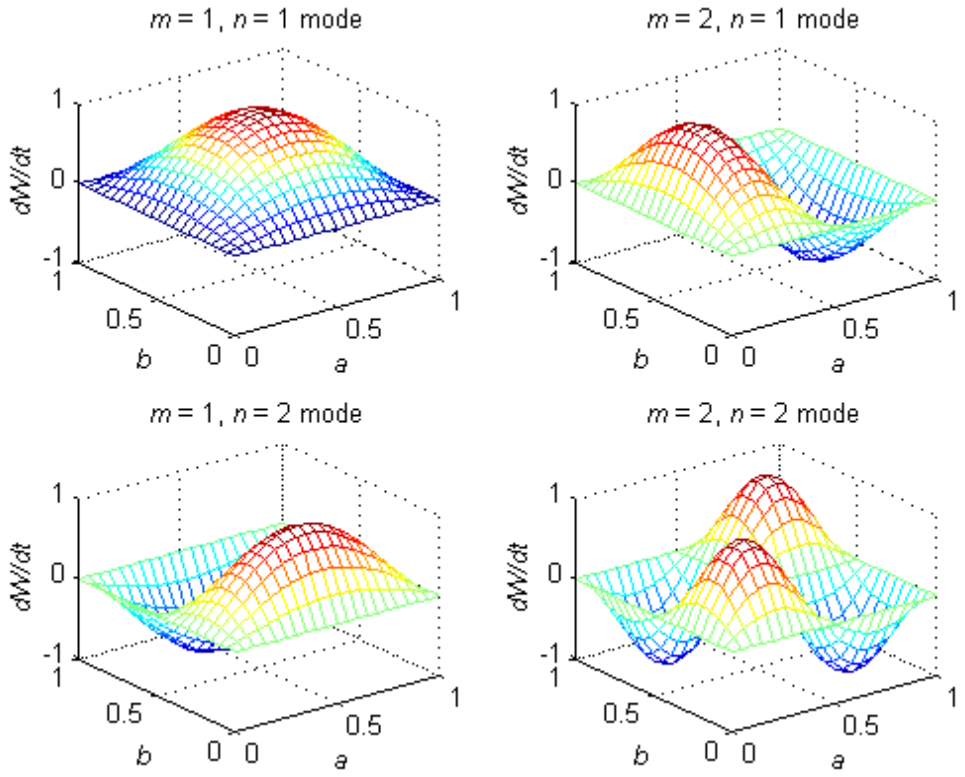

Figure 4-1: The first four theoretical velocity mode shapes of a square plate with normalized length and width dimensions: Unity Amplitude Case.

For this study let the maximum amplitude be unity and the x and y lengths be unity. Using the m=3, n=2 mode in this study, the partial derivatives in each of the directions will be unique. Figure 4-2 shows the analytical velocity mode shape and the partial derivatives of the m=3, n=2 mode. The partial derivatives are shown in Fig. 4-2, so the reader can visually verify them against the slopes of the velocity mode shape.

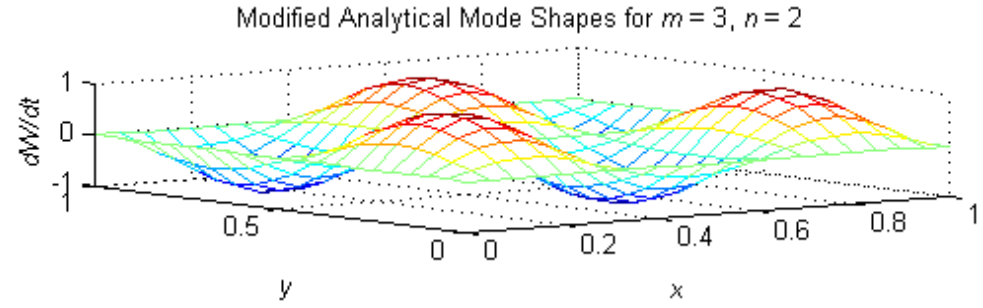

(a)

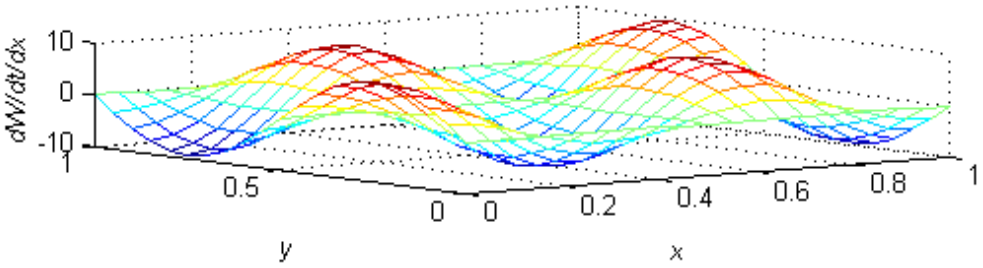

(b)

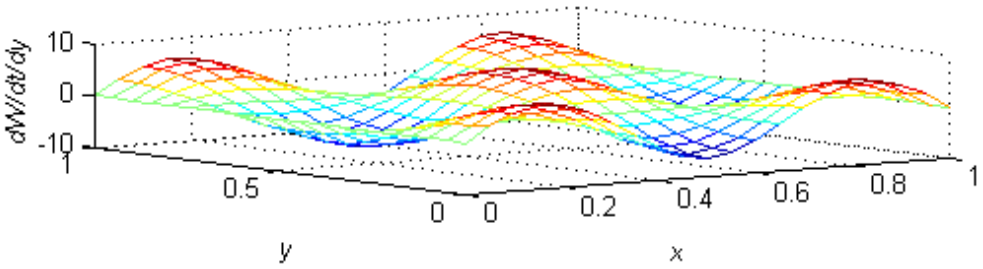

(c)

Figure 4-2: The (a) m=3, n=2 velocity mode shape of a completely simply supported rectangular plate with unity length and width dimensions, with unity amplitude, and with the partial derivatives taken in both the (b) x and (c) y directions.

Next, using the velocity data from this model, partial derivatives are taken using the DFT-IDFT approach that was discussed in chapter three. In this thesis, MATLAB® code is used to perform the partial derivatives, which incorporates the DFT-IDFT approach along each array in the direction of interest. These results can be compared to the analytical results that were displayed in Fig. 4-2. The results of these partial derivatives

with respect to the *x* and *y* directions, using the DFT-IDFT method, are shown in Figs. 4-3 and 4-4, respectively. These figures show the partial derivatives of the completely simply supported plate. Note that the error is in the neighborhood of 10^{-14} compared to maximum slope values of about 5.0. This results in an average error of the partial derivative with respect to the *x* direction of $6.4(10)^{-13}$%, a small error.

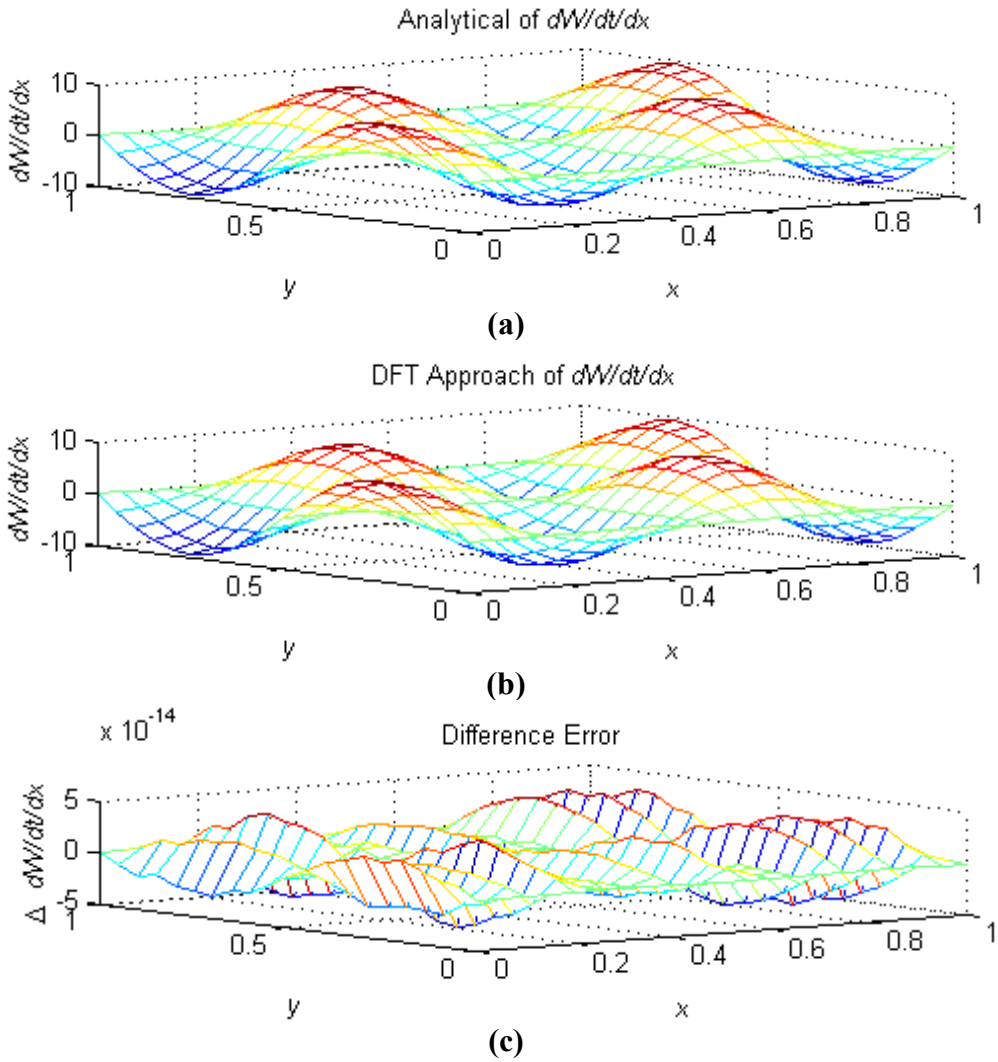

Figure 4-3: The (a) Analytical partial derivative with respect to the x direction of the *m*=3, *n*=2 velocity mode shape of a completely simply supported rectangular plate with both unity length and width dimensions and unity amplitude as compared to the (b) DFT-IDFT approach. (c) Shows the difference of the analytical versus the DFT-IDFT approach.

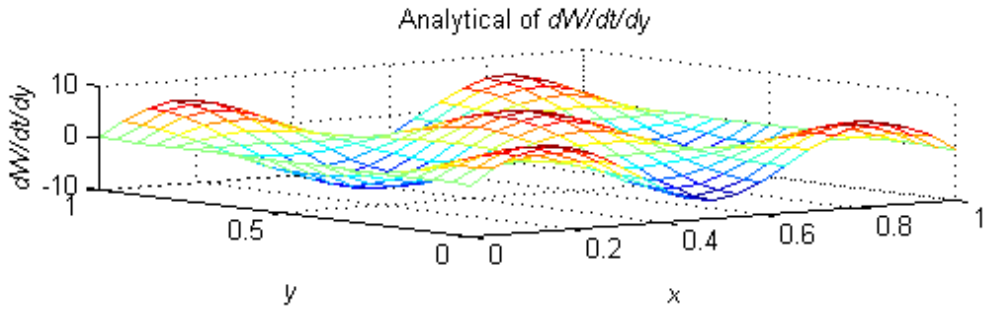

(a)

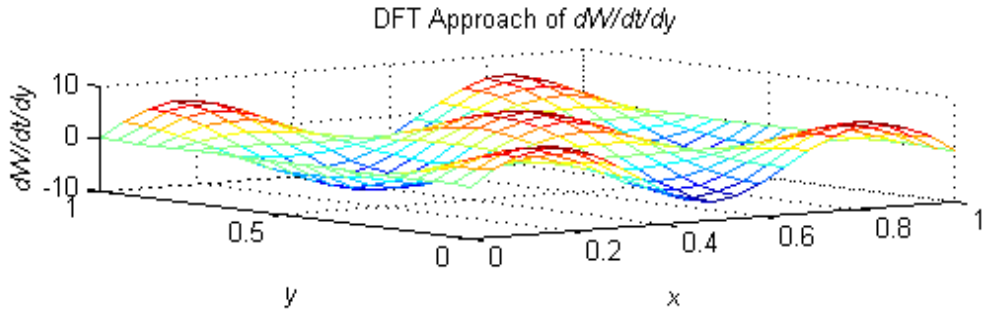

(b)

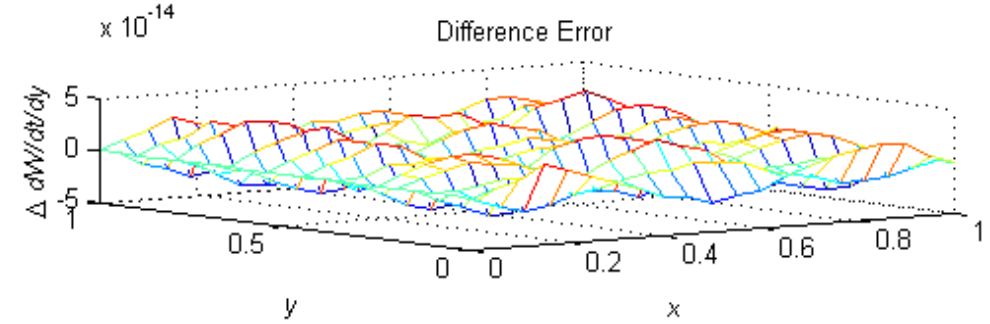

(c)

Figure 4-4: The (a) Analytical partial derivative with respect to the *y*-direction of the *m*=3, *n*=2 velocity mode shape of a completely simply supported rectangular plate with both unity length and width dimensions and unity amplitude as compared to the (b) DFT-IDFT approach. (c) Shows the difference of the analytical versus the DFT-IDFT approach.

However, what is needed is the angular data. The angular data is twice the curl of the vector field as modified Eq. (3.2) shows:

$$\boldsymbol{\theta} = \frac{1}{2}\left(\frac{\partial V_z}{\partial y} - \frac{\partial V_y}{\partial z}\right)\boldsymbol{i} + \frac{1}{2}\left(\frac{\partial V_x}{\partial z} - \frac{\partial V_z}{\partial x}\right)\boldsymbol{j} + \frac{1}{2}\left(\frac{\partial V_y}{\partial x} - \frac{\partial V_x}{\partial y}\right)\boldsymbol{k} \tag{4.5}$$

In this example data set, the velocity data is not given in the *x* and *y* directions so the angular data about the *z*-axis will be ignored. The author does not know of an experimental way to directly measure velocity through the plate thickness. It was determined in Chapter 3, Section 1., Eqs. (3.23 & 3.24), that the in-plane velocity gradient through the thickness is equal to the negative of the normal velocity gradient in the in-plane direction. Applying this theory to a plate, the following identities are formed:

$$\frac{\partial V_y}{\partial z} = -\frac{\partial V_z}{\partial y}; \quad \frac{\partial V_x}{\partial z}_y = -\frac{\partial V_z}{\partial x} \tag{4.6}$$

This reduces Eq. (4.5) to:

$$\dot{\theta}_x = \frac{\partial V_z}{\partial y}; \quad \dot{\theta}_y = -\frac{\partial V_z}{\partial x} \tag{4.7}$$

Therefore, the partial derivatives are the angular velocities with the exception of the minus sign for the angular velocity about the *y* axis.

4.1.1. Non Periodic Data

The DFT-IDFT method of partial derivatives appears to be a good algorithm to determine angular data. There are several problems though. The data analyzed in Fig. 4-2 was spatially periodic so when the algorithm makes the data periodic as described in chapter 3 it is not necessary to shear the data since the endpoints' amplitude and slope are equal.

To demonstrate the problems of non-periodic data Eq. (4.2) will be modified such that the amplitude and slope of the endpoints along the *y*-direction will not be equal. Doing this we can see the effects of shearing. This typically can be done as follows:

$$\dot{W}_{mn} = B_{mn} \sin\frac{m\pi x}{a} \sin\left(0.8\frac{n\pi y}{b}\right) \tag{4.8}$$

Truncating the data spatially in one direction can illustrate what can happen if one could only take data on a portion of a surface. This could be due to part of the surface being hidden from the laser viewpoint. This data set could also resemble an operating shape at an off resonance frequency.

Now, unlike the last example, where periodization occurs in both spatial directions, there will need to be a shearing of the Eq. (4.8) data prior to mirroring and flipping the data in the y direction. When this is performed, the endpoints, from taking a partial derivative in the y direction, show a significant error. The figures show the error occur in the midpoint, but this is truly the endpoint of the original function prior to the flipping and mirroring. From here on out the center of the figure will be termed the endpoint. In Fig. 4-5 the results of the partial derivative of the data with respect to the y direction on the non-periodic data set can be seen. (Note: The partial derivative in the x-direction is not shown, due to the fact that it would yield results the same as previous example.)

Figure 4-5(c) shows the difference of the analytical partial derivative and the DFT-IDFT method. It is difficult to express graphically the percent error of the data, because some of the slopes of the original data are zero, which would lead to a division by zero. To show how significant the error, the last row of difference data was calculated to be an error of 19.4% of the true value and the second to the last row was in error by 21.9% of the true value. The remaining data, where there was not a division by zero, averaged an error of 0.272%. The last two rows of data show a significantly larger error than the rest of the data.

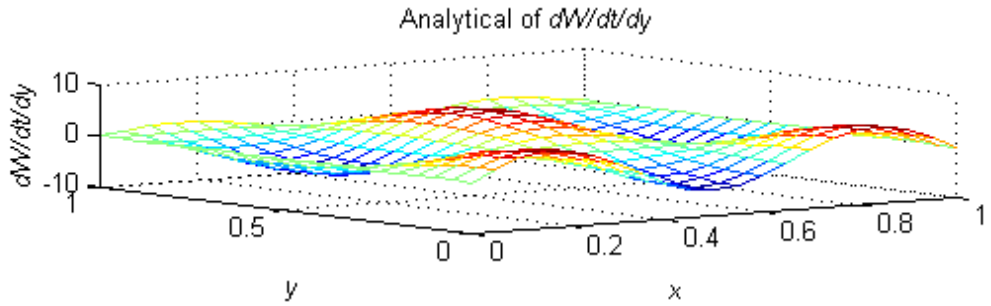

(a)

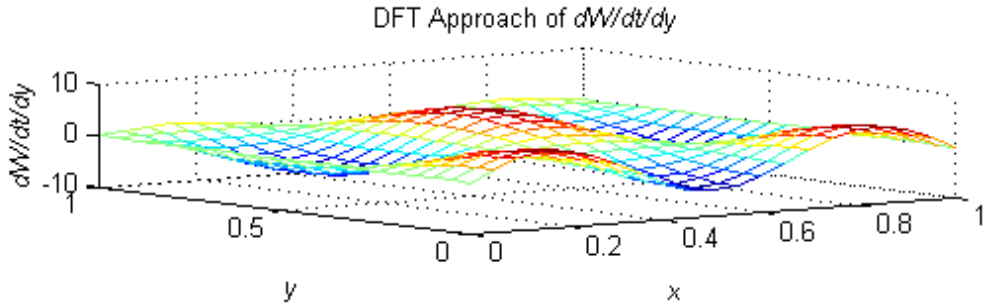

(b)

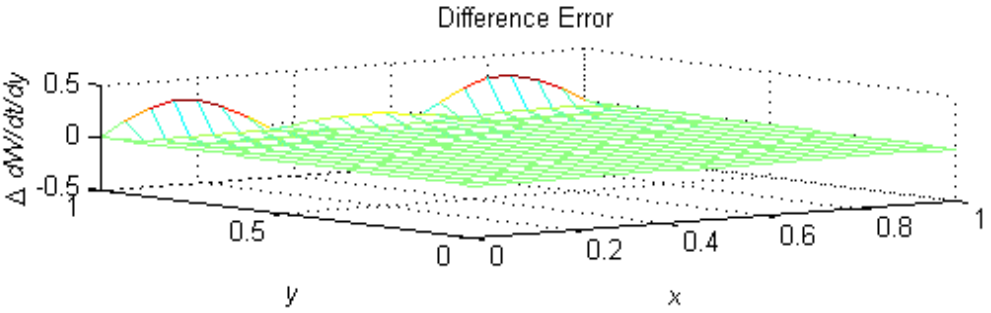

(c)

Figure 4-5: The (a) analytical partial derivative with respect to the y direction of the modified non-periodic m=3, n=2 velocity mode shape of a completely simply supported rectangular plate with both unity length and width dimensions and unity amplitude as compared to the (b) DFT-IDFT approach. (c) Shows the difference of the analytical versus the DFT-IDFT approach.

Why is the end-point error so much larger than the error on rest of the data? It is difficult to answer this question with this 2-D vibration-field example. The error can be investigated by taking a slice of this 2-D example. For this discussion we will use the slice of data at x = 0.25 as shown in Fig. 4-6(a). Figure 4-6(b) and (c) demonstrates the operation of making the data periodic. The mirrored and flipped operation increases the

number of points from 21 to 40 points, since the 21st and the 1st points are not repeated in the mirror operation.

Figure 4-7 shows the derivative of this transformed data set as compared to the DFT-IDFT derivative. The end-point difference error of 0.3015 corresponds to a 19.4% error. It is not clear as to why there is such an error with the DFT-IDFT method. The answer lies in how well the DFT describes the original equation that has been sheared prior to making it periodic. Fourier guarantees that the original data points will be reconstructed exactly, but not the points in between the original data points. The information in-between the original data points is what determines the slope (or derivative) of the data

The spectral components from the DFT of the 40 sheared, mirrored and flipped data points can be used to reconstruct points in-between the 40 data points. This DFT reconstruction is shown in Fig. 4-8(a) as compared to exact solution. In this example the equations were evaluated at a y spacing of 0.005 rather that the original 0.05 to demonstrate the error the DFT reconstruction has at points between the original points. Note that one cannot see the difference between the analytical and the DFT-IDFT partial derivative results! To eliminate this visualization problem the difference error (difference between the analytical partial derivatives and the DFT-IDFT partial derivatives) is developed and is seen in Fig. 4-8(b). This difference is not very large but when the derivative is taken the error occur over small spatial distances thus compounding the slope estimation errors. This error is largely due to a missing spectral component in the DFT reconstruction. When a DFT is taken of a finite set of data, the number of real and imaginary components must be equal to the number of original data points. When the DFT calculates the DC (cosine of the zero frequency) then it loses one of the possible 40 spectral components of the reconstruction. Thus, when the DFT reaches the Nyquist frequency ($f_N = 1/2\ f_S$), then there is only one spectral component yet to be evaluated. That spectral component is the cosine term of the Nyquist frequency, therefore the sine component at the Nyquist is missing in the DFT reconstruction.

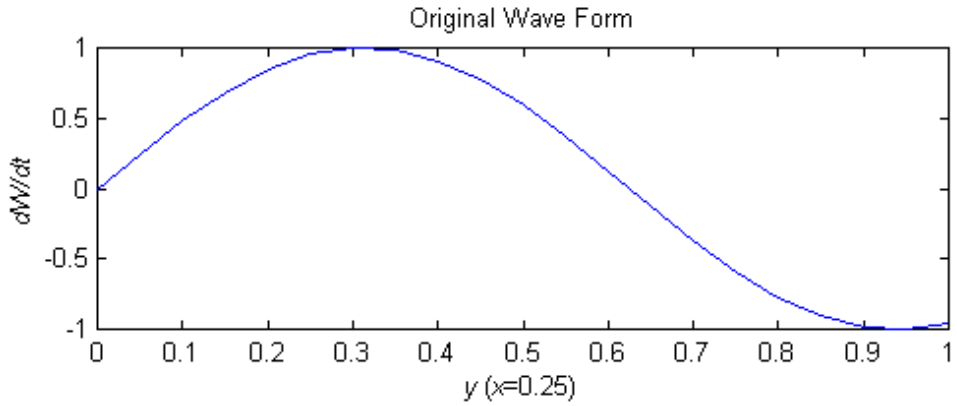

(a)

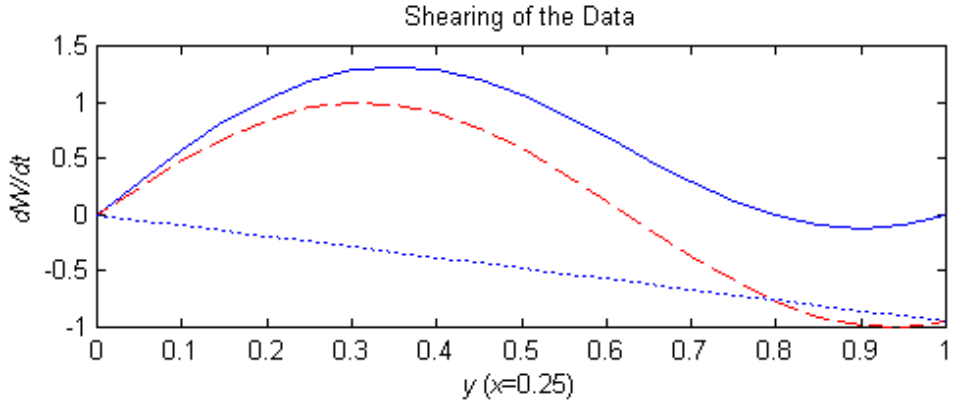

(b)

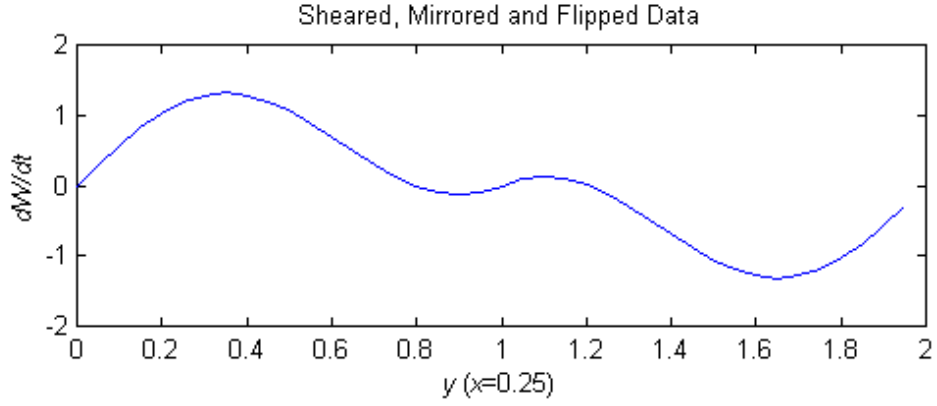

(c)

Figure 4-6: (a) A slice of the data used in Fig. 4-5 where x=0.25 (b) which is sheared (c) then mirrored and flipped.

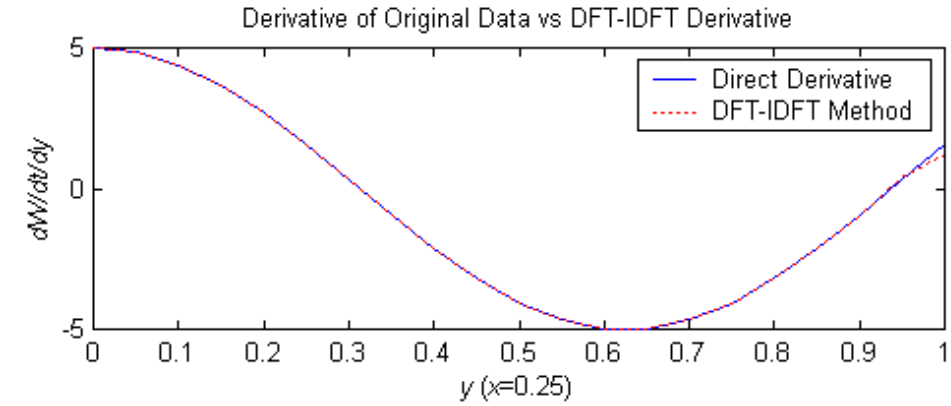

(a)

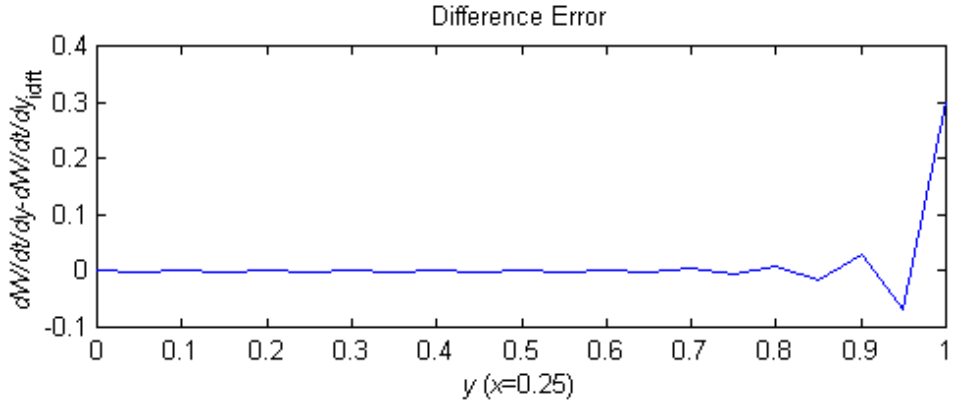

(b)

Figure 4-7: (a) The partial derivative of the exact equation compared to the derivative of DFT-IDFT method of the data used in Fig. 4-5 where x=0.25 (b) and the difference error between the two.

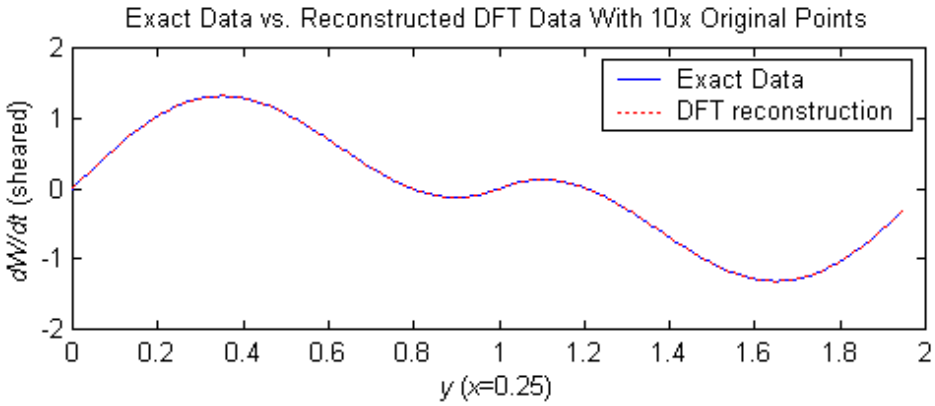

(a)

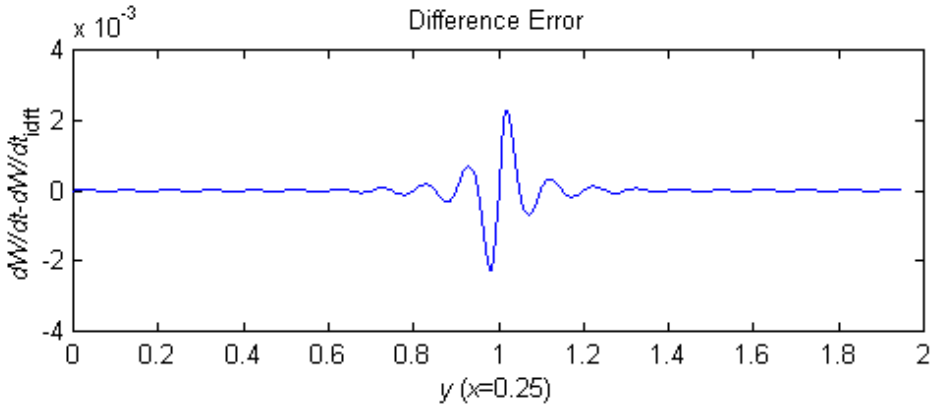

(b)

Figure 4-8: (a) The sheared, mirrored and flipped data used in Fig. 4-5 where x=0.25 as compared to the reconstructed DFT-IDFT of the data at points in-between the original data (b) and the difference error of the two.

One of the features of the laser system is the fact that it can take large amounts of spatial data rapidly. So when the same non-periodic data set in Fig. 4-5 is increased from 21 original points ($\Delta x,\Delta y$ = 0.05) to 101 points ($\Delta x,\Delta y$ = 0.01), the number of spatial frequencies, when transformed, increases by nearly five. The result of the highly sampled data set can be seen in Fig. 4-9. The error in the last row of the 101-point case is 3.87%. The error in the second to the last row is 1.04%. In the remaining data, where there is not a division by zero the error averaged 0.035%. With nearly a five-fold increase in data points the error is more than a five-fold decrease in value for the last two rows. Figure 4-10 repeats the difference error for the 101-point case. This is to be compared to the 21-point case shown in Fig 4-8(b). This demonstrates a 1/20th reduction in difference error with the increase in the number of points.

The trade-off for increased data and spectral lines results in increased computational time, which with today's computing power is probably negligible.

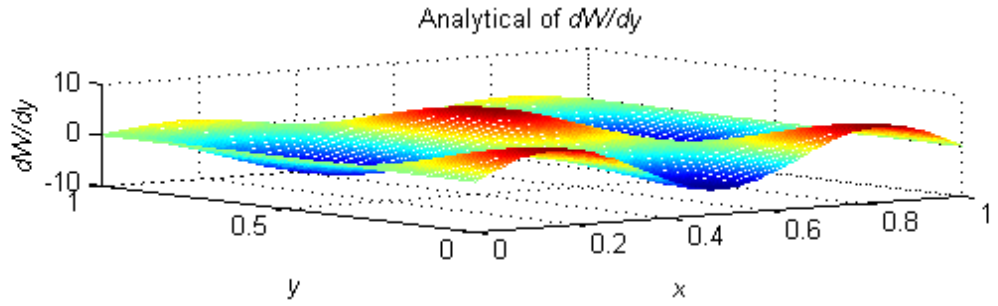

(a)

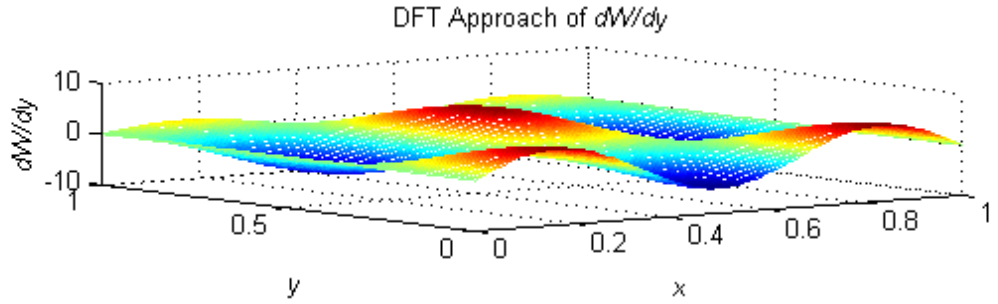

(b)

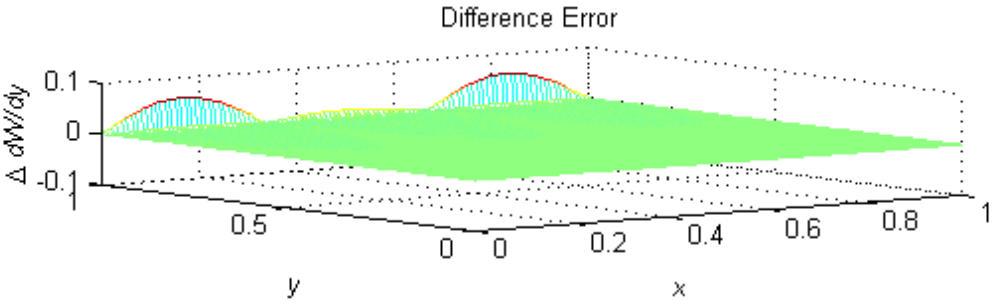

(c)

Figure 4-9: A repeat of Fig. 4-5 with an increase of data points along each direction from 21 to 101. (a) The analytical partial derivative with respect to the *y*-direction of the modified non-periodic m=3, n=2 mode shape of a completely simply supported rectangular plate with both unity length and width dimensions and unity amplitude as compared to the (b) DFT-IDFT approach. (c) Shows the difference of the analytical versus the DFT-IDFT approach.

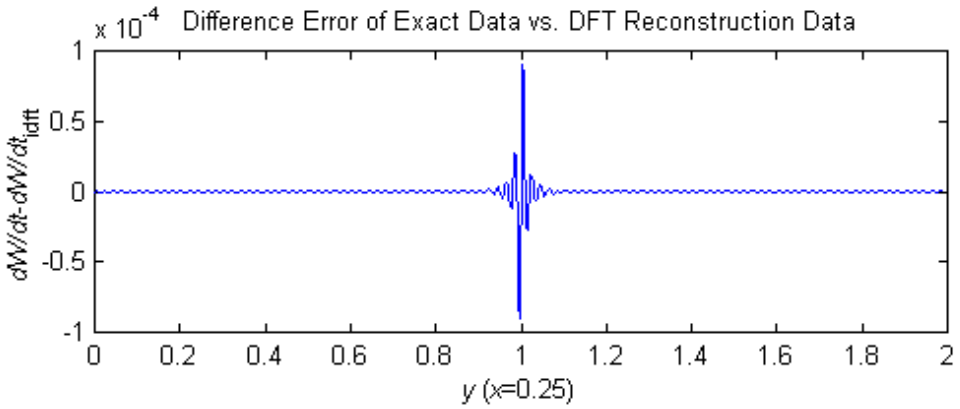

Figure 4-10: The exact analytical sheared, mirrored and flipped data used in Fig. 4-8 with increasing the number of original points from 21 to 101 as compared to the reconstructed DFT-IDFT with both evaluated at points in-between the original data point spacing.

4.1.2. Noisy Data

Noise is present when working with experimental data. This noise can be contributed to electrical noise, laser dropout, quantization error, etc. With this in mind, the same case study is useful when studying noise present in the data. The non-periodic data in the y-direction, as used in the previous section, will be more interesting than the periodic data. Using the MATLAB® m-file already created from the previous example, random noise can be added as 2% and 5% of the maximum amplitude. With the use of normal probability distribution of the random number generator in MATLAB®, and unity amplitude of the data, random data is added with three standard deviations totaling 0.02 and 0.05, respectively

In Fig. 4-11 the original data is shown with noise added of three standard deviations totaling 0.02. Figures. 4-12 and 4-13 show the results of the difference between the theoretical partial and the DFT-based partial derivative techniques in both of the x and y directions. Both partial derivatives are shown to demonstrate the effects of noise on a periodic non-sheared partial derivative (with respect to x) and a partial derivative (with

respect to *y*) of data that was sheared to make it periodic. The error of the partial derivative with respect to *x* is 9.8%, excluding divide by zero error. The error with respect to y, excluding the last two rows is 20.7%. When looking at the last two rows there is a maximum error of 147.3% in the last row and 679.0% in the second to the last row. (Note: These percent values vary with new runs of the same code due to the nature of random noise generator.)

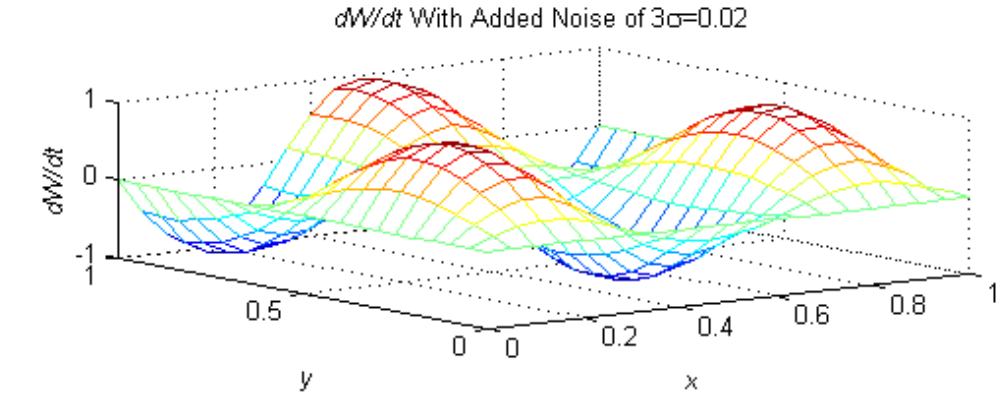

(a)

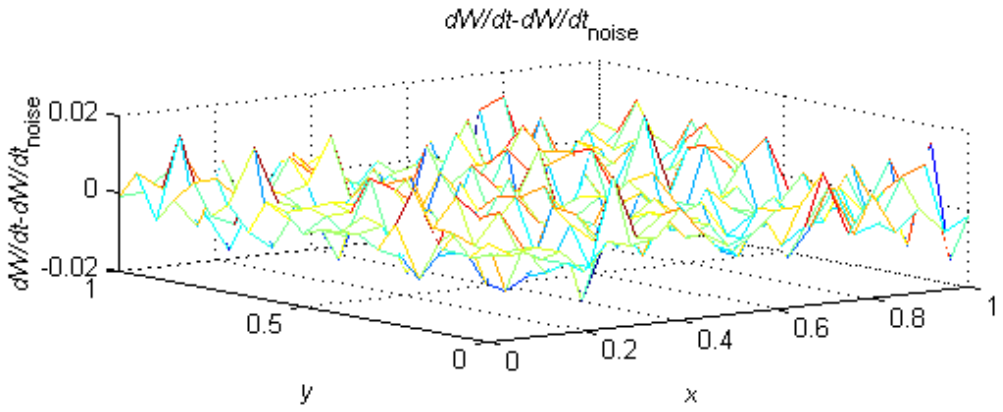

(b)

Figure 4-11: The (a) modified m=3, n=2 velocity mode with added noise of three standard deviations of 0.02 and the (b) noise distribution.

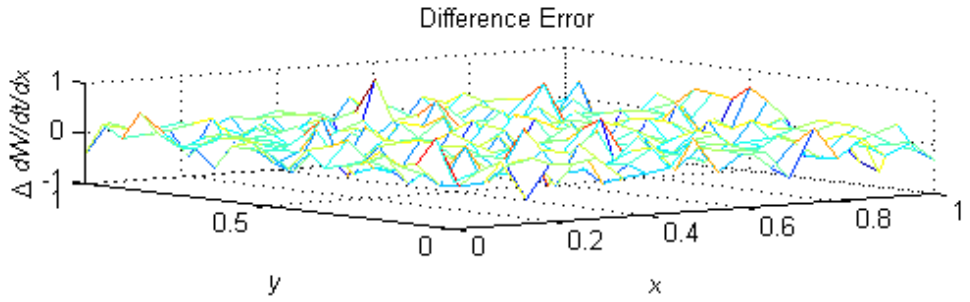

Figure 4-12: The difference error of the two partial derivative techniques with respect to *x* of the modified *m*=3, *n*=2 velocity mode with added noise of three standard deviations of 0.02.

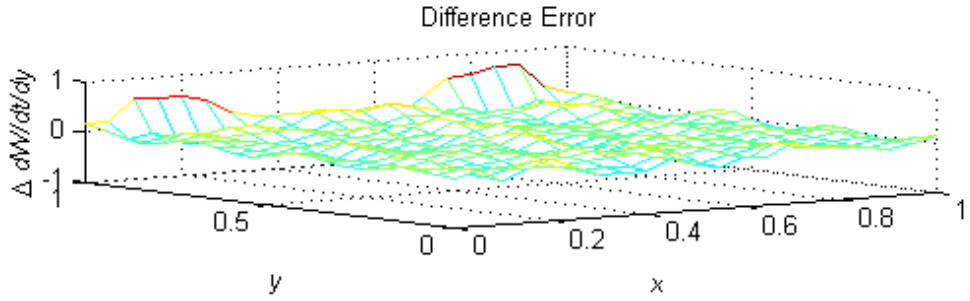

Figure 4-13: The difference error of the two partial derivative techniques with respect to *y* of the modified *m*=3, *n*=2 velocity mode with added noise of three standard deviations of 0.02.

These are significantly large errors. Looking at the study of Neumann [4], a method of reducing these large errors is to remove higher frequency components when transforming back to the spatial domain. When reducing the frequencies to the first 40% of the spectral lines, which are the first 8 of the 20 frequencies available, the errors are reduced as summarized in Table 4-1.

Table 4-1: Table of percent error of partial derivatives of adding 3 standard errors totaling 0.02 with $\Delta=0.05$

	% error of d*W*/dt/d*x*	% error of d*W*/dt/d*y* excluding last two rows	Max % of last row of d*W*/dt/d*y*	Max % of 2nd to last row of d*W*/dt/d*y*
All frequencies	9.8	20.7	147.3	679.0
1st 40% of spatial freqs.	2.6	5.7	67.5	311.2

Table 4-2 shows the percent of error when adding three standard deviations with an error totaling 0.05. Without filtering high frequencies, the second to the last row of data is found to have an error value that is more than an order of magnitude in error. Filtering out high frequencies does prove to be an advantage in reducing the error. The data can re-simulated at a higher spatial resolution of $\Delta=0.01$ for the same noise of 0.05. This can be demonstrated in Table 4-3. The first 8 spatial frequencies were kept which was 8% of the frequency lines. The filtering of the partial derivative in the y direction can be seen in Fig. 4-14. The unfiltered data (Fig. 4-15) there is no recognizable pattern, just noise. This shows that the higher spectral lines are capturing the noise.

Table 4-2: Table of percent error of partial derivatives of adding 3 standard errors totaling 0.05 with $\Delta=0.05$

	% error of d*W*/dt/d*x*	% error of d*W/dt*/d*y* excluding last two rows	Max % of last row of d*W/dt*/d*y*	Max % of 2nd to last row of d*W/dt*/d*y*
All frequencies	21.9	60.5	477.5	2472.7
1st 40% of spatial freqs.	7.1	16.0	109.2	186.5

Table 4-3: Table of percent error of partial derivatives of adding 3 standard errors totaling 0.05 with Δ=0.01

	% error of d*W*/dt/d*x*	% error of d*W*/dt/d*y* excluding last two rows	Max % of last row of d*W*/dt/d*y*	Max % of 2nd to last row of d*W*/dt/d*y*
All frequencies	247.9	296.7	13257	8959.2
1st 8% of spatial freqs	6.5	27.8	528.3	638.4

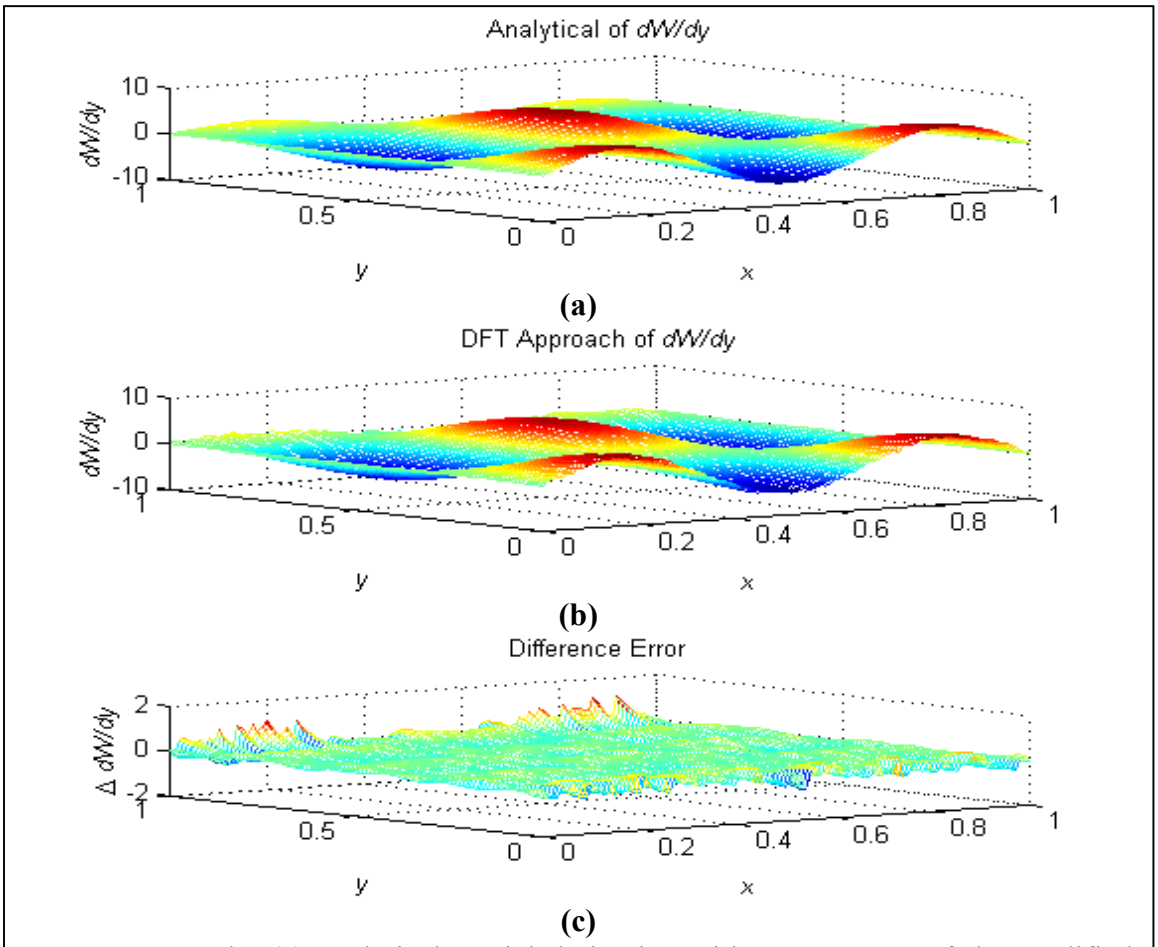

Figure 4-14: The (a) analytical partial derivative with respect to *y* of the modified *m*=3, *n*=2 velocity mode and Δ=0.01. (b) The DFT-IDFT partial derivative method with respect to *y* of the same function with the addition of three standard deviations of noise totaling 0.05, then filtering out the high frequency components keeping the first eight spectral lines. (c) The difference error.

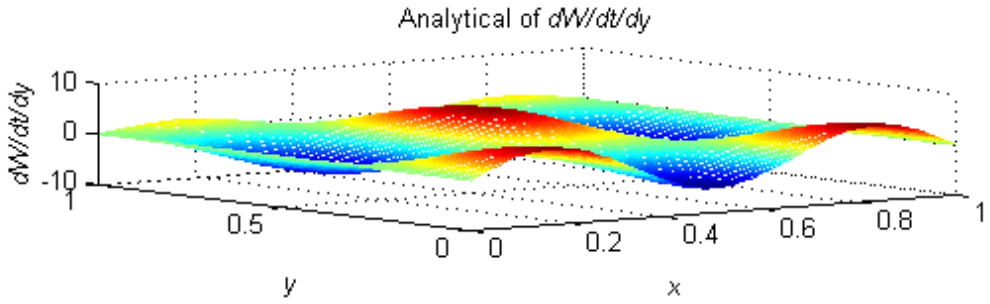

(a)

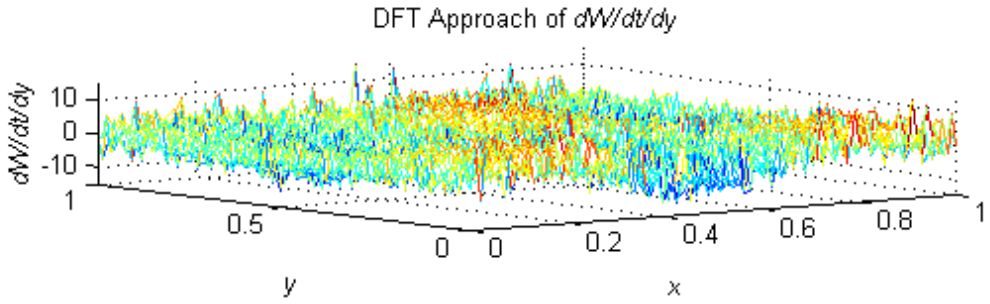

(b)

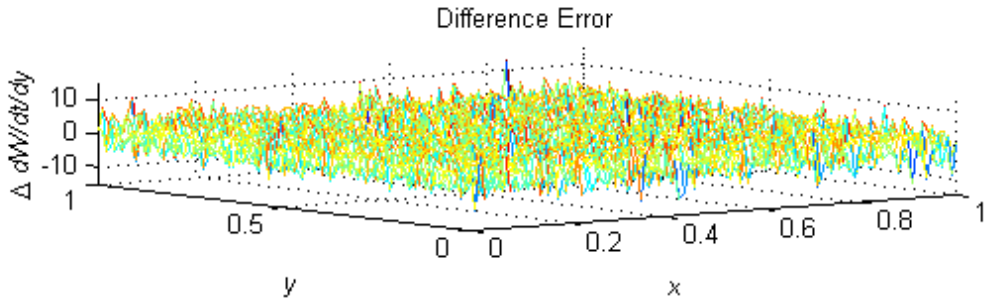

(c)

Figure 4-15: The (a) analytical partial derivative with respect to y of the modified m=3, n=2 velocity mode and $\Delta(x,y)$=0.01 (b) The DFT-IDFT partial derivative method with respect to y of the same function with the addition of three standard deviations of noise totaling 0.05. (c) The difference error.

In summary, the more spatial frequencies kept the less error in reconstruction in the absence of noise. When noise is present in the data, the fewer the spectral lines used the better the fit. The trade off made in filtering out the higher spectral lines, is still the end points of non-periodic data. To reduce the endpoint error more spatial sampling of the laser can be performed. As a rule of thumb, in spectral filtering, Sun and Mitchell [34] use five times the spatial waves present in the data. In this data set the *x* direction has 1.5 spatial waves and the *y* direction has 0.8 spatial waves, which would lead to 7.5 and 4 spatial frequencies, respectively.

4.2. In-Plane Modes

In order to demonstrate the drilling modes or angular velocities about the out-of-plane axis the in-plane vibrations are needed. Equation (4.5) described this earlier. One analytical case study that that is useful is the Lamé modes as described by Lloyd [45]. Galaitsis [33] used the Lamé mode equations. These will be used here.

The theory of Lamé, describes the in-plane motion for thin-rectangular plates with totally free boundary conditions. The plate is free from restrictions in the in-plane directions, which allows it to vibrate in plane. Here defined, the corners of the Lamé modes of thin-rectangular plates has zero displacement in both the *x* or *y*-axis direction. The two geometric shapes for which the Lamé mode equations are developed are for the square plate and the rectangle plate in which the sides are at a 3:1 ratio. These are depicted in Fig. 4-16.

Galaitsis [33] with the aid of Lloyd [45] gives the equations for the displacement of the square isotropic thin plates as:

$$D_x = C \sin\left(\frac{\pi x}{L_x}\right)\cos\left(\frac{\pi y}{L_y}\right) \tag{4.5}$$

$$D_y = -C \cos\left(\frac{\pi x}{L_x}\right)\sin\left(\frac{\pi y}{L_y}\right) \tag{4.6}$$

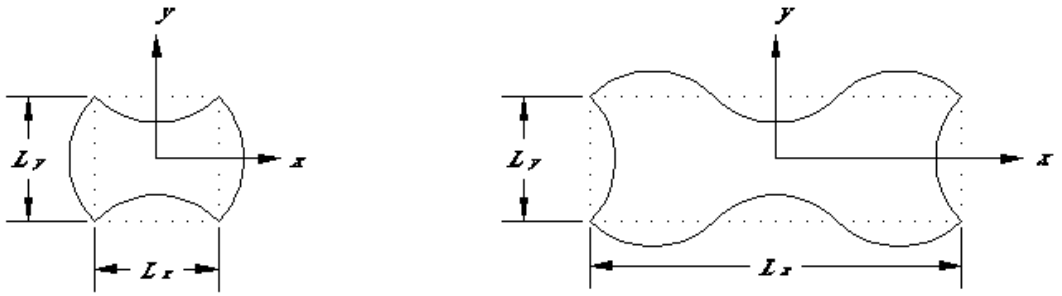

(a) (b)

Figure 4-16: The Lamé mode shapes for the (a) square plate and (b) the 3:1 aspect ratio. (As modified from Galaitsis [33])

where D_x and D_y is the displacement in the x and y direction respectively, C is a constant and $L_y/L_x = 1$. The natural frequency is:

$$f_n = \frac{0.5}{L}\sqrt{\frac{E}{\rho(1+\upsilon)}} \tag{4.7}$$

The similar equations for a rectangular isotropic thin plate of 3:1 aspect ratio have been shown by Lloyd [47] to be:

$$D_x = C\sin\left(\frac{3\pi x}{L_x}\right)\cos\left(\frac{\pi y}{L_y}\right) \tag{4.8}$$

$$D_y = -C\cos\left(\frac{3\pi x}{L_x}\right)\sin\left(\frac{\pi y}{L_y}\right) \tag{4.9}$$

$$f_n = \frac{3}{2L_x}\sqrt{\frac{E}{\rho(1+\upsilon)}} \tag{4.10}$$

where $L_x/L_y = 3$.

From this point on, the 3:1 rectangular isotropic thin plate will be used to demonstrate the angular velocity about the z-axis. The derivative of the displacement field with respect to time is required to get the angular velocity. This can be achieved by

multiplying Eqs. (4.8) and (4.9) by $j\omega$ (where $\omega = 2\pi f_n$). The velocity field can be described in Eqs. (4.11) and (4.12) using $C_1 = j\omega C$.

$$V_x = C_1 \sin\left(\frac{3\pi x}{L_x}\right)\cos\left(\frac{\pi y}{L_y}\right) \tag{4.11}$$

$$V_y = -C_1 \cos\left(\frac{3\pi x}{L_x}\right)\sin\left(\frac{\pi y}{L_y}\right) \tag{4.12}$$

By normalizing Eqs. (4.11) and (4.12) and by allowing $L_x = 3$ and $L_y = 1$ and $C_1 = 1$, the velocity field is simulated as seen in Fig. 4-17. To obtain the end result of angular velocity, the partial derivatives in the spatial domain needs to be taken as shown in Eqs. (4.13) and (4.14). The spatial derivatives are displayed in Fig. 4-18.

$$\frac{\partial V_x}{\partial y} = -\frac{\pi}{L_y} C_1 \sin\left(\frac{3\pi x}{L_x}\right)\sin\left(\frac{\pi y}{L_y}\right) \tag{4.13}$$

$$\frac{\partial V_y}{\partial x} = \frac{3\pi}{L_x} C_1 \sin\left(\frac{3\pi x}{L_x}\right)\sin\left(\frac{\pi y}{L_y}\right) \tag{4.14}$$

Since the spatial derivatives are periodic in space, the DFT-IDFT method can be performed on the velocity field with an outcome of essentially zero error. This was shown previously. The resulting partial derivatives are now used in the angular velocity equation, Eq. (4.5). This equation is then reduced to Eq. (4.15) for angular velocity about the z-axis. The angular velocity about the z-axis is shown in Fig. 4-19.

$$\omega_z = \frac{1}{2}\left(\frac{\partial V_y}{\partial x} - \frac{\partial V_x}{\partial y}\right)\boldsymbol{k} \tag{4.15}$$

In summary, this chapter demonstrates the use of the DFT-IDFT technique to generate a source functionalization, which can have its partial derivatives taken and then the partial derivatives are used to obtain the angular velocities in the structure. Both examples given in this chapter were assumed to be excited with a single-frequency sinewave tuned to a resonance frequency. In real data at any arbitrary frequency you may be off-resonance and, thus, have an operating shape that is a superposition of all of the structural modes.

The only problem is that any of the structural modes shapes that have a spatial waveform that is greater than the spatial Nyquist frequency will be poorly represented and can be aliased as a lower spatial frequency. Just like in time domain data, we can apply a low pass filter to filter out higher spatial frequency data. This, of course, must be done prior to the DFT-IDFT process. MATLAB® has the capability to low pass filter using several filtering techniques (i.e. n^{th} order Butterworth or Chebyshev). It will be recommended in chapter 6 that the use of filters should be studied if needed for experimental data.

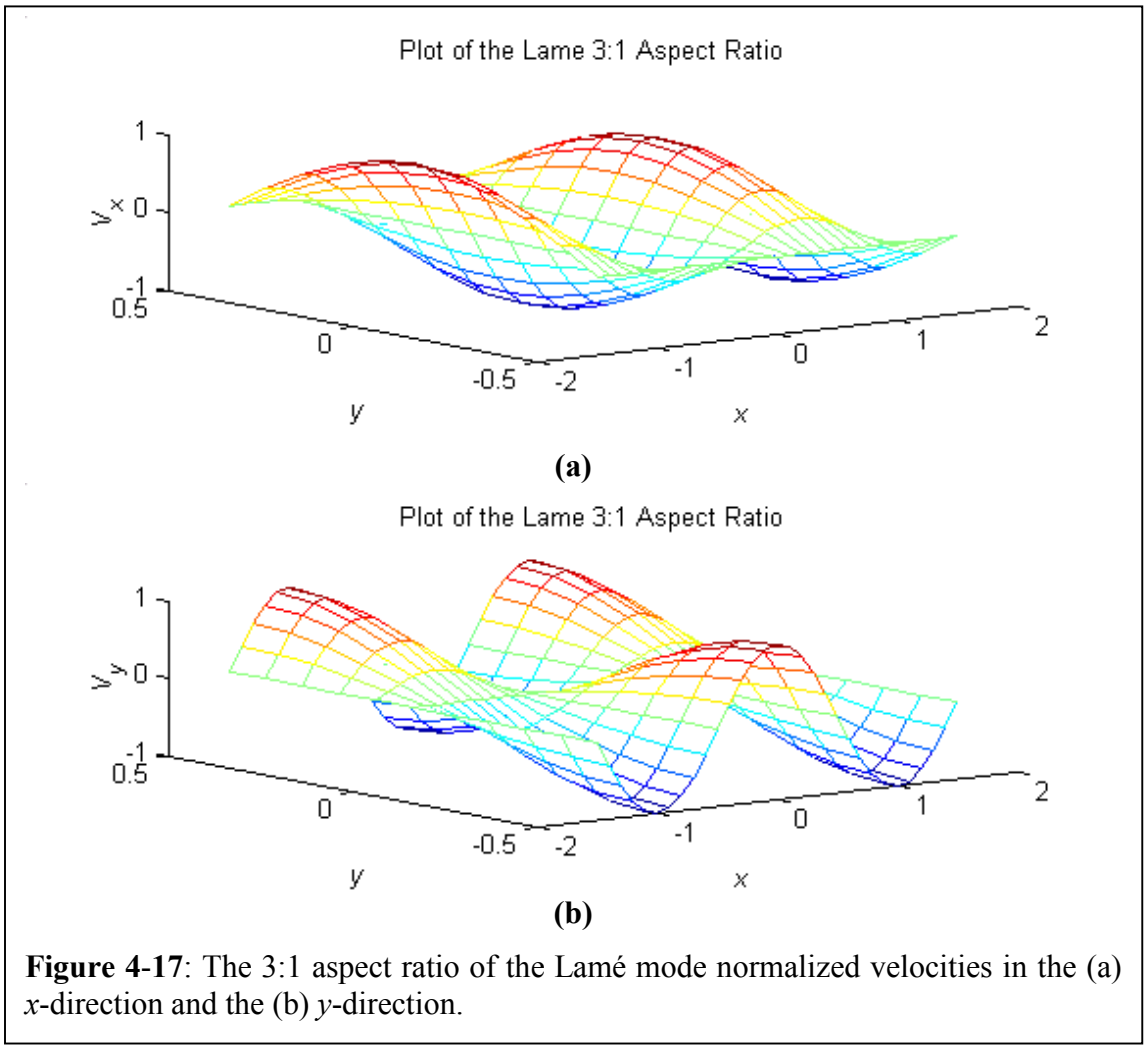

Figure 4-17: The 3:1 aspect ratio of the Lamé mode normalized velocities in the (a) *x*-direction and the (b) *y*-direction.

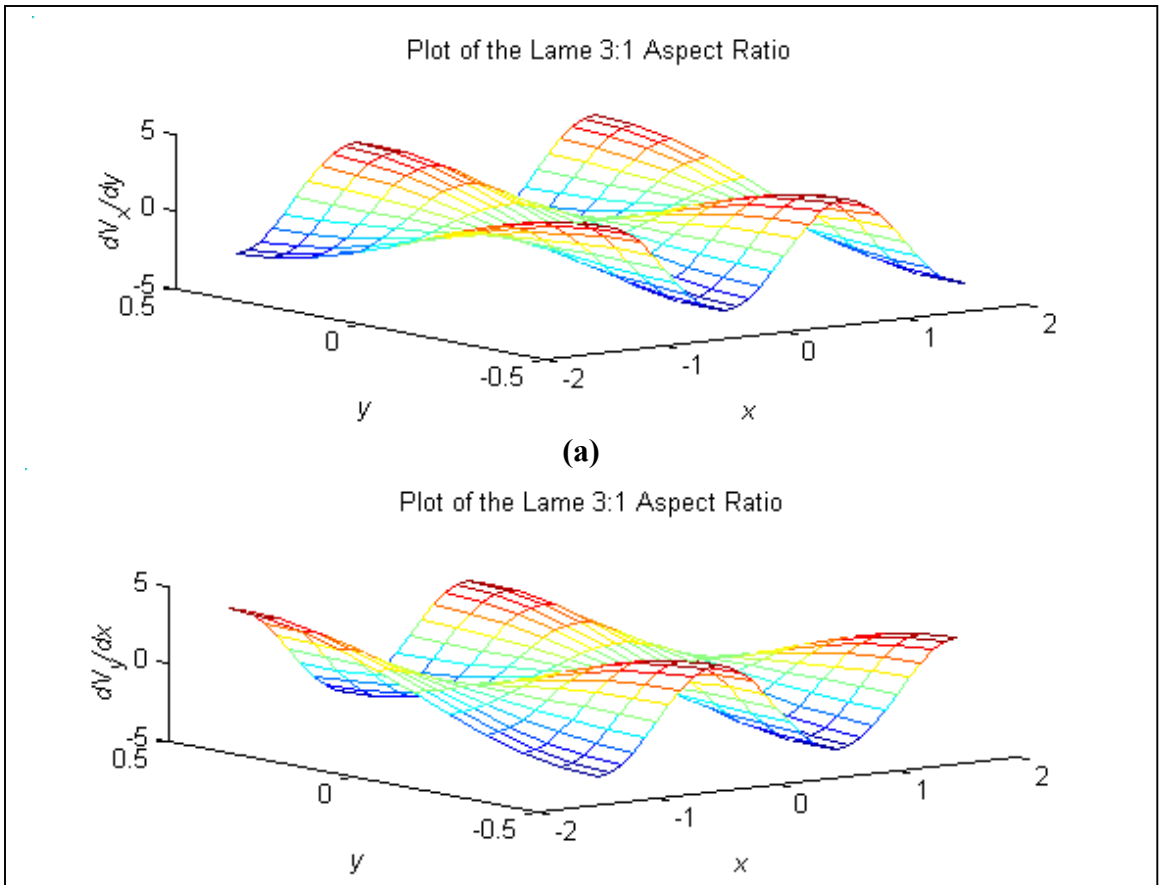

Figure 4-18: The partial derivatives of the 3:1 aspect ratio of the Lamé mode normalized velocities in the (a) *x*-direction with respect to *y* and the (b) *y*-direction with respect to *x*.

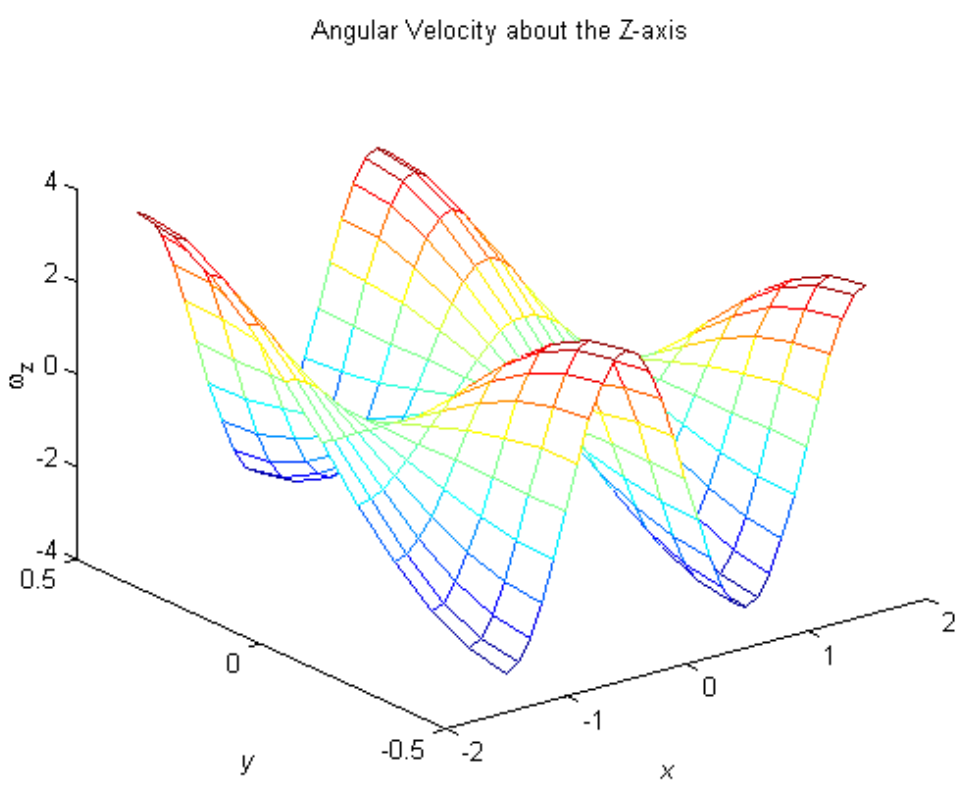

Figure 4-19: The 3:1 aspect ratio of the Lamé mode with curl of the normalized velocity field to obtain ω_z.

Chapter 5

A Proposed Experimental Verification Procedure

In this chapter, a method will be proposed in which the laser-based angular velocity extraction technique could be evaluated against an accelerometer-based method of measuring angular velocity.

5.1. A Method of Experimental Verification

It is proposed that Kistler Translational-Angular PiezoBEAM® (TAP®) accelerometers be used to measure the translational and rotational accelerations of a structural installation. The TAP® accelerometers are to be arranged in a triaxial configuration. The data set from these accelerometers should provide a set of three translational accelerations and a set of three rotational accelerations. These accelerations can be integrated in the frequency domain to their corresponding translational and rotational velocities. Theoretically these velocities can be compared to the translational and rotational velocities obtained from the laser-based methods at the same, single point on the structure where the Triaxial TAP® accelerometer system is attached. Figure 5-1

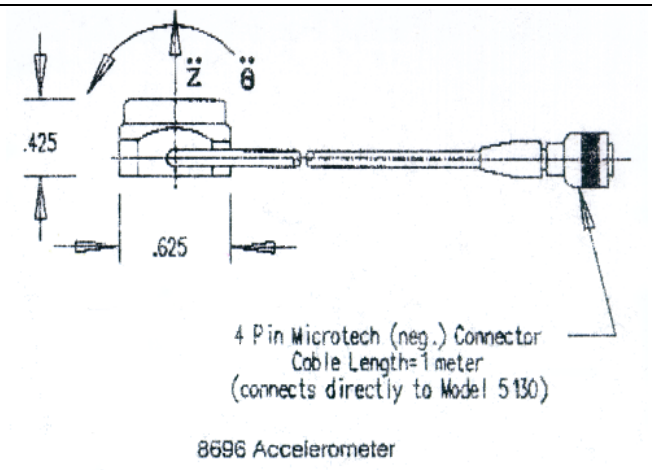

Figure 5-1: A sketch of a Kistler 8696 TAP® accelerometer. (After the Type 8832 technical bulletin, Kistler Instrument Corporation, Amherst, NY. [46])

shows a side-view sketch of one of these TAP® accelerometers. The accelerometer can measure the outward, normal acceleration to its mounting surface and the angular acceleration about a second axis dependant upon direction of mounting. The operation of this accelerometer is through the use of two piezoelectric ceramic beams mounted as seen in Fig 5-2. When undergoing pure linear acceleration the beams are in phase with each other. When the beams are in pure angular motion, they are out of phase. Any combination of the two will produce two complex signals, which the signal processor unit will separate into its two measurement directions. (Note: In Fig. 5-1 Kistler has used the second derivative of z. In this chapter we will switch from u,v,w notation for 3-D translational coordinate displacements to x,y,z for representing motion about the three directions. This has been done for consistency with the Kistler figures used here.)

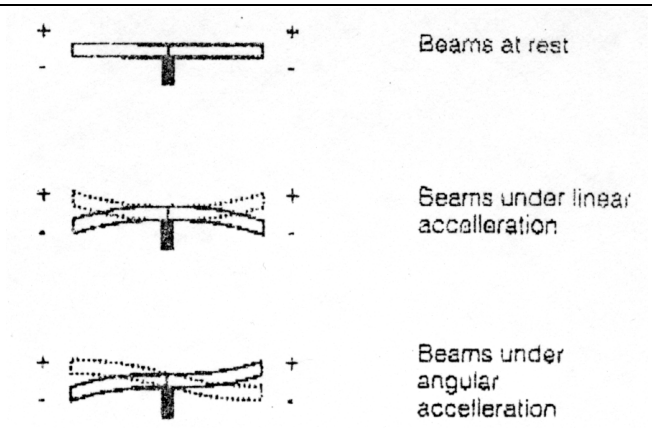

Figure 5-2: A sketch of a the pair of cantilever beams inside of a Kistler 8696 TAP® accelerometer.(After Figure 1 of Type 8832 technical bulletin, Kistler Instrument Corporation, Amherst, NY. [46])

Production of a triaxial configuration requires a precision-mounting block. The block must be made such that both the three linear acceleration axes and the three angular acceleration axes are perpendicular. Figure 5-3 shows the drawing that might be submitted to the shop for manufacturing of this block. Figure 5-4 depicts the arrangement of the three accelerometers mounted on the block. Close scrutiny of Fig. 5-4 shows that the TAP® accelerometers will not measure the true translational accelerations of the structure's surface due to their offset from the mounting surface or more precisely, the

translational accelerometer sees the true translation plus the rotationally induced acceleration in the direction of the accelerometer's sensing axis. Thus, an engineering analysis of this triaxial installation must be made in order to extract the true translational accelerations.

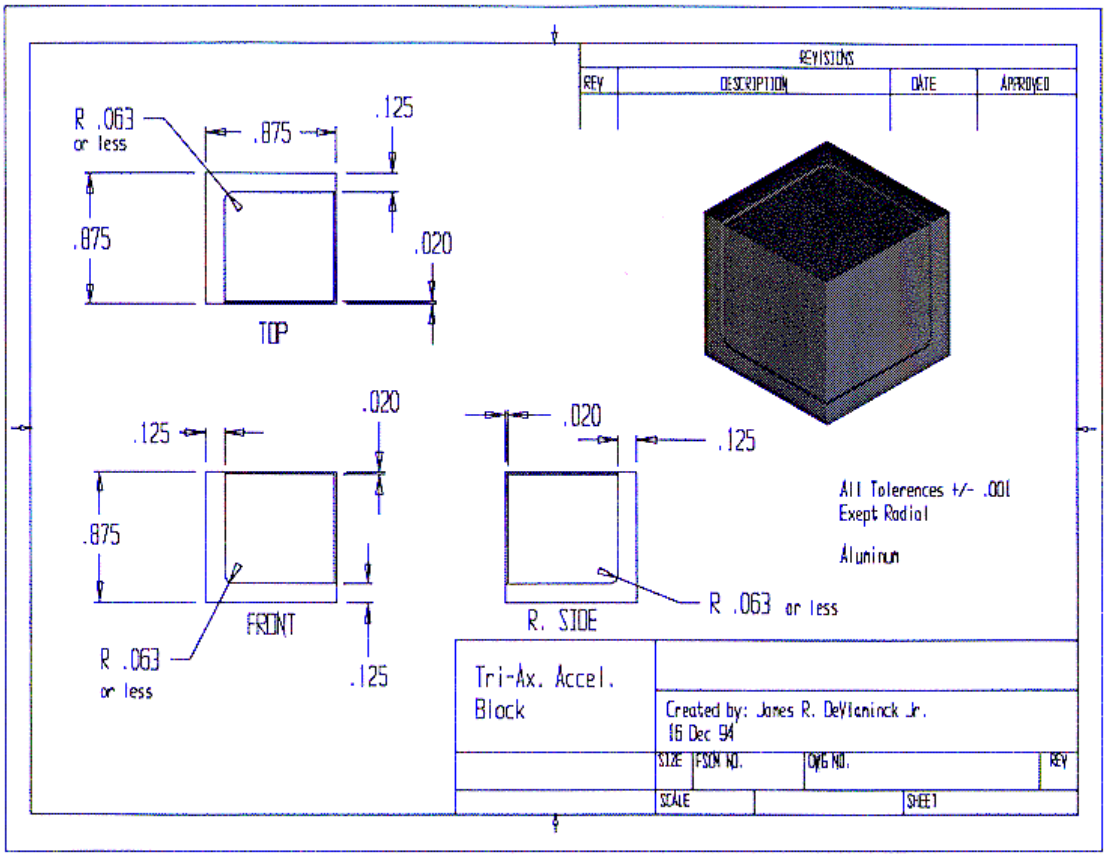

Figure 5-3: A drawing of the mounting block used to mount three Kistler TAP® accelerometers orthogonally.

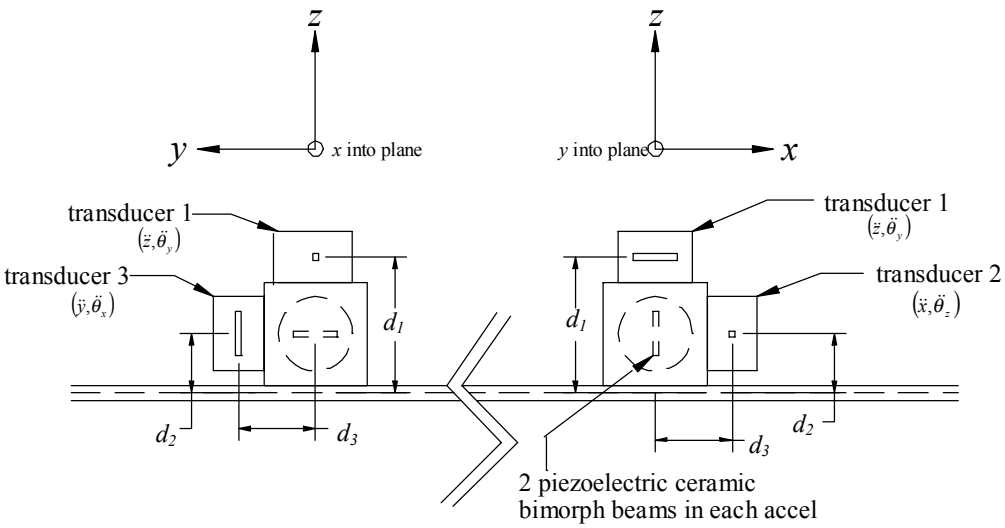

Figure 5-4: A diagram depicting a triaxial arrangement of Kistler TAP® accelerometers to be used in conjunction with Table 5-1.

In first analyzing Fig. 5-4 it was theorized that the three accelerometers could make incorrect measurements due to cross-axis sensitivity, centripetal accelerations or rotational acceleration-induced translational accelerations due to the transducer's position being at a distance away from the surface of the structure. Table 5-1 reviews all of the components that contribute to the accelerations seen by the TAP® triaxial accelerometer system. At this time do not try to interpret the entries in the table. The various entries will be described below.

Table 5-1: This table is to be used in conjunction with Fig 5-3 to show all the possible contamination of the measured signals.

Measured Values	Phenomenon that may contaminate the measured values in obtaining actual values	Comments
transducer 1 $\ddot{z}$	$\ddot{y}$ bending about z-axis	Cross-axis sensitivity
	$d_1\ddot{\theta}_x$ bending about z-axis	Cross-axis sensitivity
	$d_1\dot{\theta}_y^{\,2}$ centripetal acceleration -bending about y-axis	Possible components at DC and $2\omega_f$
	$d_1\dot{\theta}_x^{\,2}$ centripetal acceleration -bending about y-axis	Possible components at DC and $2\omega_f$
$\ddot{\theta}_y$	$\ddot{\theta}_z$ bending about z-axis	Cross-axis sensitivity
	$\ddot{x}$ axial tension and compression of beams	Cross-axis sensitivity
	$d_1\ddot{\theta}_y$ axial tension and compression of beams	Cross-axis sensitivity
transducer 2 $\ddot{x}$	$\ddot{z}$ bending about x-axis	Cross-axis sensitivity
	$d_3\ddot{\theta}_y$ bending about x-axis	Cross-axis sensitivity
	$d_2\ddot{\theta}_y$ bending about z-axis	
	$d_3\dot{\theta}_z^{\,2}$ centripetal acceleration -bending about z-axis	Possible components at DC and $2\omega_f$
	$d_3\dot{\theta}_y^{\,2}$ centripetal acceleration -bending about z-axis	Possible components at DC and $2\omega_f$
$\ddot{\theta}_z$	$\ddot{\theta}_x$ bending about x-axis	Cross-axis sensitivity
	$\ddot{y}$ axial tension and compression of beams	Cross-axis sensitivity
	$d_3\ddot{\theta}_z$ axial tension and compression of beams	Cross-axis sensitivity
transducer 3 $\ddot{y}$	$\ddot{x}$ bending about y-axis	Cross-axis sensitivity
	$d_3\ddot{\theta}_z$ bending about y-axis	Cross-axis sensitivity
	$d_2\ddot{\theta}_x$ bending about x-axis	
	$d_3\dot{\theta}_z^{\,2}$ centripetal acceleration –bending about x-axis	Possible components at DC and $2\omega_f$
	$d_3\dot{\theta}_x^{\,2}$ centripetal acceleration –bending about x-axis	Possible components at DC and $2\omega_f$
$\ddot{\theta}_x$	$\ddot{\theta}_y$ bending about x-axis	Cross-axis sensitivity
	$\ddot{z}$ axial tension and compression of beams	Cross-axis sensitivity
	$d_3\ddot{\theta}_x$ axial tension and compression of beams	Cross-axis sensitivity

To demonstrate how the different terms of Table 5-1 were developed, let us take transducer 1, which is the transducer that measures linear acceleration in the *z* direction and the angular accelerations about the *y*-axis. Figure 5-5 is shown in order to give visual reference when discussing these terms. First, acceleration in the *y* direction would subject the two piezoBEAMS® to in-phase bending about the *z*-axis. This would result in a cross-axis sensitivity term added to the *z* acceleration. The next term is the *y*-direction tangential acceleration of the transducer caused by locating the accelerometer at a distance, d_1, from the surface of the structure ($d_1\ddot{\theta}_x$). This too would give a cross-axis sensitivity term added to the *z* acceleration. Centripetal accelerations of the forms, $d_1\dot{\theta}_y{}^2$ and $d_1\dot{\theta}_x{}^2$, would subject the two piezoBEAMS® to in-phase bending about the *y*-axis, which is not a cross-axis sensitivity.

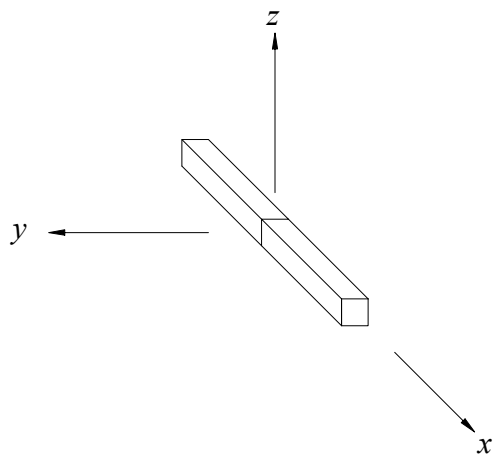

Figure 5-5: A sketch depicting the piezoBEAMS® within transducer 1, to aid in discussion of how the measured values may be contaminated.

The angular accelerations about the z-axis give the two beams cross-axis out-of-phase signals, which can contaminate the angular accelerations of the transducer about the y-axis. Accelerations of $\ddot{x}$ and $d_1\ddot{\theta}_y$ both subject the two beams to axial tension and compression, which are out-of-phase cross-axis signals of the beams as well. This cross-axis sensitivity will contaminate the angular acceleration about the *y*-axis. The

phenomena that may contaminate the other two transducers' measured values are left as an exercise to the reader.

It was determined by talking to a Kistler engineer (Mike Inslako [47]), that any cross-axis sensitivity terms are less than 1% of the major axis acceleration. Therefore, it would not be too alarming to remove these terms, since they likely do not have a significant impact to the measurement error.

In this research, it is proposed that the structure is excited at a single frequency. The linear accelerations that are contaminated by centripetal accelerations are at twice forcing frequency. As the transducer moves through one complete angular displacement, it experiences two cycles of linear displacement. Figure 5-6 was created to aid in visualizing how angular motion of the accelerometer under centripetal motion results in

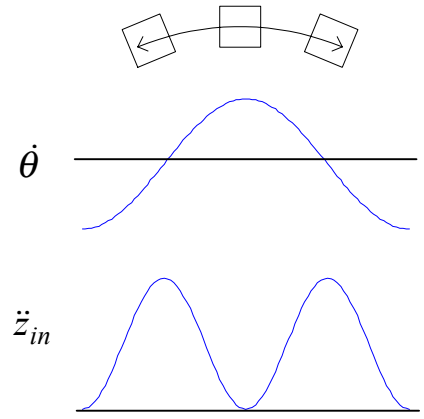

Figure 5-6: An illustration demonstrating how linear displacement of an accelerometer will occur at twice the rate (or frequency) of its angular position as it undergoes a centripetal motion.

the linear vibration changing at a rate (or frequency) of twice the angular motion. Therefore, there are two remaining terms of the twenty-three terms in Table 5-1 that are used to correct the measured acceleration values. The final corrected acceleration equations are as follows:

$$\ddot{z} = \ddot{z}_m \tag{5.1}$$

$$\ddot{\theta}_y = \ddot{\theta}_{ym} \tag{5.2}$$

$$\ddot{x} = \ddot{x}_m + d_2\ddot{\theta}_{ym} \tag{5.3}$$

$$\ddot{\theta}_z = \ddot{\theta}_{zm} \tag{5.4}$$

$$\ddot{y} = \ddot{y}_m - d_2\ddot{\theta}_{xm} \tag{5.5}$$

$$\ddot{\theta}_x = \ddot{\theta}_{xm} \tag{5.6}$$

where the subscript *m* denotes the measured value and the subscripts in *x, y* and *z* represent the axes about which the accelerations are measured. These acceleration values can then be integrated (or multiplied by $1/i\omega_f$) to obtain the velocity values that are the result of the laser measurements and the angular velocity calculations.

5.2. A Second Method for Experimental Verification

If we look further at the centripetal accelerations a second method in obtaining a check of the angular velocity information can be shown. Let us take the centripetal accelerations and break them down in their generic form. First,

$$\dot{\theta} = \Omega \cos \omega_f t \tag{5.7}$$

where ω_f is the forcing frequency and then Ω is the rotational velocity amplitude. Then centripetal accelerations can be expressed as:

$$r \times \dot{\theta} \times \dot{\theta} = r\Omega^2 \cos^2 \omega_f t \tag{5.8}$$

through trigonometric identities the equation can be rewritten as:

$$r \times \dot{\theta} \times \dot{\theta} = r\Omega^2 \left(\frac{1 + \cos 2\omega_f t}{2} \right) \tag{5.9}$$

In the previous section we discuss how the centripetal accelerations occurred at DC and at twice the forcing frequency. Equation (5.9) mathematically proves that discussion.

We can now develop a system of equations evaluating the linear accelerations of the triaxial set of TAP® accelerometers at either the DC component or at twice the forcing frequency. For those who are experienced at the use of piezoelectric accelerometers it is known that data is not very accurate at the zero frequency line. For this study we will

look at the values at twice the forcing function. The system of equations can be written as:

$$\ddot{z}(2f) = \frac{d_1 \Omega_y^{\,2}}{2} + \frac{d_1 \Omega_x^{\,2}}{2} \tag{5.10}$$

$$\ddot{x}(2f) = \frac{d_3 \Omega_y^{\,2}}{2} + \frac{d_3 \Omega_z^{\,2}}{2} \tag{5.11}$$

$$\ddot{y}(2f) = \frac{d_3 \Omega_x^{\,2}}{2} + \frac{d_3 \Omega_z^{\,2}}{2} \tag{5.12}$$

These systems of equations can, therefore, be solved for to obtain the rotational velocities:

$$\Omega_x = \sqrt{\frac{\ddot{z}(2f)d_3 - \ddot{x}(2f)d_1 + \ddot{y}(2f)d_1}{d_3 d_1}} \tag{5.13}$$

$$\Omega_y = \sqrt{\frac{\ddot{z}(2f)d_3 + \ddot{x}(2f)d_1 - \ddot{y}(2f)d_1}{d_3 d_1}} \tag{5.14}$$

$$\Omega_z = \sqrt{\frac{-\ddot{z}(2f)d_3 + \ddot{x}(2f)d_1 + \ddot{y}(2f)d_1}{d_3 d_1}} \tag{5.15}$$

These equations provide a second check of the rotational velocities at a single point on a structure.

This chapter has provided two methods to experimentally measure rotational velocities to compare to the analytical derivatives of laser data. The next chapter will summerize the work of this thesis and provide recommendations for further studies.

Chapter 6

Conclusions and Recommendations

This chapter will summarize the work that has been developed and demonstrated in this thesis. Recommendations for future work conclude this chapter.

6.1 Summarization of the Thesis Work

In this research, it was shown that there was a need for experimentally determining angular vibration data in order to compare, to help update, and to verify the analytical solutions of finite element models. There have been methods developed by researchers like Stanbridge et al. [24] that measure in-plane angular vibration, which lacks the "drilling modes" (or the angular velocities about the out-of-plane axis). With the solution described in this thesis, all three angular vibration directions along with the linear data are obtained with one method using a laser-based data acquisition system. This will aid in correlating with the six degree-of-freedom solutions that finite element methods obtain.

The curl function was taken of the velocity field. The curl was found to be related to desired angular vibration information. The DFT-IDFT method of taking derivatives was demonstrated in this thesis. The method first curve fits the data with a Fourier transform then partial derivatives are taken on the transform result to obtain the needed information for the determination of the in-plane and out-of-plane angular velocities.

Analytical examples of the out-of-plane and in-plane vibrations were used to validate the DFT-IDFT method. The effects of non-periodic data and noisy data were demonstrated using these analytical examples. The use of Sun and Mitchell's [35] spectral filtering to reduce the effects of noise proved to be quite effective on reducing the noise-induced error. Lastly, an experimental verification procedure was proposed to check the developed laser-based rotational velocity extraction technique.

6.2 Recommendations for Future Work

There are areas in which this research can be further molded in order to understand if there are better or more refined methods of obtaining the angular vibration data from laser-based, 3-axis translational vibration data. These would consist of the following topics.

- Study the application of the curl theory to curved plates and shells.
- Study other curve fitting techniques with respect to:
  - The handling of non-periodic data.
  - The handling of noise, laser dropouts, etc.
- Study the applications of low-pass spatial filter to filter out higher order spatial frequencies above about 80% of the Nyquist frequency.
- Study the ways of directly measuring through plate thickness.

6.2.1. Curved plates

The discussions at the end of chapter 3 show the use of parametric space to deal with curved plates. This is a tool that is commonly used in finite elements and could very well be applied here. The question is when using the mechanic of materials example that was developed in chapter 3, the through plate thickness derivatives were equal to the negative of the in-plane derivatives. What is the conversion of this relationship to applications in parametric space? How does one handle the conversion back to geometric space? An equivalent through plate thickness derivatives relation will have to be developed.

6.2.2. Other Curve Fitting Techniques

There are many other methods in which to curve fit the linear velocity data. These can be polynomial equations with a least squares or spline fits. Further work can be done to compare the different methods as to how well do they deal with fitting the data and how they perform the differentiation of the data. Whether it can only handle perfect data, non-periodic data, noisy data, edge points, or any other problems that are associated with taking derivatives with non-perfect solutions. The other methods can compare simple

analytical known solutions like that in chapter 4. Statistics can be use to evaluate the various methods of curve fitting to determine which curve fit can best handle most vibration patterns one would most likely come across.

6.2.3. Low-Pass Spatial Filter

This research did not take into consideration the real chance that experimental data may include higher frequency spatial mode shapes that are not properly captured in the spatial resolution available. Spatial aliasing may occur. It is suggested to further study applying a low-pass spatial filter to filter out higher spatial frequencies beyond the Nyquist spatial frequency.

6.2.4. Measuring Through-Thickness Vibration Data

This is mentioned since the mechanics of material solution in chapter 3 shows that the through thickness derivative is equal to the in-plane derivative for the case of beams. This is based upon the assumption that the strains are linear throughout the thickness of the beam (i.e. small displacements). For most cases, the small deflection situation can be controlled with a controllable input. But, this is not always true.

Developing other non-contacting measuring tools in which the full three degree of freedom vibration pattern can be measured not only on the surface of the structure, but also throughout the thickness, could prove to be useful. It is not known if such a method exists. Could this be done through the use of ultrasonic waves? This is presented to provoke thought into the next generation of measuring vibration in the non-contacting world.

References

[1] Zeng, X., *The Estimation and Statistical Inferences of the Position and Orientation of a Scanning Laser Doppler Vibrometer*, Ph.D. Dissertation, Virginia Polytechnic Institute and State University, Department of Mechanical Engineering, Blacksburg, VA, November 1994.

[2] Zeng, X., A. L. Wicks, and L. D. Mitchell, "The Determination of the Position and Orientation of a Scanning Laser Vibrometer for a Laser-Based Mobility Measurement System", *Proceedings of the First International Conference on Vibration Measurements by Laser Techniques: Advances and Applications*, Ancona, Italy, October 3-5, 1994, pp. 81-92.

[3] Zeng, X., L. D. Mitchell, and B. L. Agee, "A Laser Position Determination Algorithm for an Automated Mechanical Mobility Measurement System," *Proceedings of the 11th International Modal Analysis Conference*, Vol. 1, Kissimmee, FL, 31 January-4 February 1993, pp. 122-129.

[4] Neumann, M. L., *A Method for the Spatial Functionalization of the Dynamic Response of a Structure with Stability Considerations*, M.S. Thesis, Virginia Polytechnic Institute and State University, Department of Mechanical Engineering, Blacksburg, VA, December 1993.

[5] Neumann, M. L., "A Method for the Spatial Functionalization of Laser-Based Dynamic Response of a Structure," *Proceedings of the 13th International Modal Analysis Conference*, Nashville, TN, 13-16 February 1995, pp. 742-748.

[6] Lopez Dominguez, J. C., *Reconstruction of 3-D Structural Dynamic Response Fields: An Experimental, Laser-Based Approach with Statistical Emphasis*, Preliminary Ph.D. Research Proposal, 7 December 1993. Available from Prof. A. L. Wicks or Prof. L. D. Mitchell.

[7] Abel, J. J., and L. D. Mitchell, "Extraction of In-Plane Velocities Using Laser Doppler Velocimetry," *Proceedings of the 11th International Modal Analysis Conference*, Vol. 1, Kissimmee, FL, 31 January - 4 February 1993, pp. 402-408.

[8] Abel, J. J., *Three-Dimensional Velocity Extraction Using Laser Doppler Vibrometry*, M.S. Thesis, Virginia Polytechnic Institute and State University, Department of Mechanical Engineering, Blacksburg, VA, 1993.

[9] Donovan, J. B., *Three-Dimensional Vibrometry Via Three Positions of a One-Dimensional Laser Doppler Velocimeter*, M.S. Thesis, Virginia Polytechnic Institute and State University, Department of Mechanical Engineering, Blacksburg, VA, 1991.

[10] Montgomery, D. E., *Modeling and Visualization of Laser-Based 3-D Experimental Spatial Dynamic Response*, Ph.D. Dissertation, Virginia Polytechnic Institute and State University, Department of Mechanical Engineering, Blacksburg, VA, to be published December 1994.

[11] Montgomery, D. E., and R. L. West, "Computer Animation of complex Modal Response of One-, Two-, and Three-Dimensional Structures*," Proceedings of the 11th International Modal Analysis Conference*, Vol. 2, Kissimmee, FL, 31 January-4 February 1993, pp. 1321-1327.

[12] Mitchell, L. D., "A Perspective View of Modal Analysis," *The International Jounal of Analytical and Experimental Modal Analysis*, Vol. 3, No. 2, April 1988, pp. 45-48.

[13] Elliott, K. B., *Structural Modification Utilizing Beam Elements*, Ph.D. Dissertation, Virginia Polytechnic Institute and State University, Department of Mechanical Engineering, Blacksburg, VA, 1985.

[14] Elliott, K. B. and L. D. Mitchell, "Structural Modification Utilizing Beam Elements," *Proceedings of the 5th International Modal Analysis Conference*, Vol. 2, London, England, 6-9 April 1987, pp. 956-965.

[15] Patton, M. E., and M. W. Trethewey, "A Survey and Assessment of Nonintrusive-Model-Testing Techniques for Ultralightweight Structures," *The International Jounal of Analytical and Experimental Modal Analysis*, Vol. 2, No. 4, October 1987, pp. 163-173.

[16] Smith, J. E., "Measurement of the Total Structural Mobility Matrix," *The Shock and Vibration Bulletin* #40, Part 7, December 1969, pp. 51-84.

[17] Ewins, D. J., and M. G. Sainsbury, "Mobility Measurement for the Vibration Analysis of Connected Structures," *The Shock and Vibration Bulletin* #42, Part 1, January 1972, pp. 105-113.

[18] Anonymous, *American National Standard Guide to the Experimental Determination of Rotational Mobility Properties and the Complete Mobility Matrix*, ANSI S2.34-1984 (ASA 34-1984), Acoustical Society of America, New York, NY, 1984.

[19] Morris, H. D., R. B. Peters, and P. H. Merritt, "A Precision Inertial Angular Vibration Measuring System," *The Shock and Vibration Bulletin* #50, Part 2, September 1980, pp. 1-10.

[20] Yasuda, C., P. J. Riehle, D. L. Brown, and R. J. Allemang, "An Estimation Method for Rotational Degrees-Of-Freedom Using a Mass Additive Technique," *Proceedings of the 2nd International Modal Analysis Conference*, Vol. 2, Orlando, Florida, 1984, pp. 877-886.

[21] Ptacnik, M., J. Lamka and I. Fort, "Velocity Vector LDA Measurement Inside a Pitched Blade Impeller." *Dantec Information*, Skovlande, Denmark, No. 12, February 1993, pp. 6-9.

[22] Taubner, A., and H-J Martens, "Devlopment and Investigation of diffraction grating interferometers," *Proceedings of the First International Conference on Vibration Measurements by Laser Techniques: Advances and Applications*, Ancona, Italy, October 3-5, 1994, pp. 145-152.

[23] Lewin, A. C., V. Roth, and G. Siegmund, "New Concept for Interferometric Measurement of Rotational Vibrations," *Proceedings of the First International Conference on Vibration Measurements by Laser Techniques: Advances and Applications*, Ancona, Italy, October 3-5, 1994, pp. 24-36.

[24] Stanbridge, A. B., and D. J. Ewins, "Measurement of Translational and Angular Vibration Using a Scanning Laser Doppler Vibrometer," *Proceedings of the First International Conference on Vibration Measurements by Laser Techniques: Advances and Applications*, Ancona, Italy, October 3-5, 1994, pp. 37-47.

[25] Tretheway, M. W., H. J. Sommer and J. A. Cafeo, "A Dual Beam Laser Vibrometer for Measurement of Dynamic Structural Rotations and Displacements," *Journal of Sound and Vibration*, Vol. 164, No. 1, 8 June 1993, pp. 67-84.

[26] Cafeo, J. A., M. W. Tretheway, and H. J. Sommer III, "On the Use of Measured Rotational Degrees-of-Freedom In Structural Dynamics Modification," *Proceedings of the 11th International Modal Analysis Conference*, Vol. 1, Kissimmee, FL, 31 January-4 February 1993, pp. 96-101.

[27] Cafeo, J. A., J. R. Rieker, M. W. Tretheway, and H. J. Sommer III, "Application of a Three Degree of Freedom Laser Vibrometer for Experimental Modal Analysis," *Proceedings of the 9th International Modal Analysis Conference*, Vol. 2, Florence,Italy, 15-18 April 1991, pp. 1161-1167.

[28] Ulcker, J. J., J. Denavit, and R. S. Hartenberg, " An Iterative Method for the Diplacement Analysis of Spatial Mechanisms," *Journal of Applied Mechanics*, ASME, Vol. 31, No. 2, June 1964, pp 309-314.

[29] Sommer III, H. J., M. J. Erickson, and M. W. Tretheway, "Single-Beam Laser Vibrometer for Simultaneous Measurement of Translation, Pitch, and Roll with Neural Network Calibration," *Proceedings of the 12th International Modal Analysis Conference*, Vol. 2, Honolulu,Hawaii, 31 January-3 February 1994, pp. 1196-1201.

[30] Bokelberg, E. H., H. J. Sommer, M. W. Tretheway, and C. H. Chu, "Simultaneous Measurement of Six Coordinate Vibration: Three Translations and Three Rotations," *Proceedings of the 11th International Modal Analysis Conference*, Vol. 1, Kissimmee, FL, 31 January-4 February 1993, pp. 522-527.

[31] Ng'andu, A. N., C. H. J. Fox, and E. J. Williams, " Estimation of Rotational Degrees of Freedom Using Curve and Surface Fitting," *Proceedings of the 11th International Modal Analysis Conference*, Vol. 1, Kissimmee, FL, 31 January-4 February 1993, pp. 620-626.

[32] Kochersberger, K., L. D. Mitchell, and A. L. Wicks, "Structural Angular Velocity Extraction Using DFT-IDFT Techniques," *Proceedings of the 9th International Modal Analysis Conference*, Vol. 1, Florence,Italy, 15-18 April 1991, pp. 657-663.

[33] Galaitsis, G. S., *Extraction of Drilling-Angular Velocities Using a Nodal-Spatial Array of In-Plane Translational Velocities*, M.S. Thesis, Virginia Polytechnic Institute and State University, Department of Mechanical Engineering, Blacksburg, VA, May 1993.

[34] Sun, F. P., and L. D. Mitchell, "Two-Dimensional Velcity Data Smoothing and Structural Angular Velocity Extraction Using a DFT-IDFT Technique," *Proceedings of the 13th Biennial ASME Conference on Mechanical Vibration and Noise*, 22-25 September,1991, pp. 303-309.

[35] Arruda, J. R. F., "Surface Smoothing and Partial Spatial Derivatives Computation Using a Regressive Discrete Fourier Series," *Mechanical Systems and Signal Processing*, 6(1), 1992, pp. 41-50.

[36] Mitchell, L. D., Personal Communication, Virginia Polytechnic Institute and State University, Randolph Hall, Room 118A, Blacksburg, VA December 6, 1994, 5:00 pm.

[37] *Webster's New World Dictionary*, Warner Books, New York, NY, 1990, p. 149.

[38] Kreyszig, Erwin, *Advanced Engineering Mathematics*, 6th Edition, John Wiley & Sons, Inc., New York, 1988 pp 46-7 & 566

[39] Ellis, Robert and Gulick, Denny, *Calculus With Analytic Geometry*, 2nd Edition, Harcourt Brace Jovanovich, Inc., New York, 1982, pg. 845-846 & 899.

[40] Ford, Hugh, *Advanced Mechanic of Materials*, 2nd Edition, Ellis Horwood Limited, Sussex, England, 1977

[41] Higdon, Archie, et. al., *Mechanics of Materials*, 4th Edition, John Wiley & Sons, Inc., New York, 1985.

[42] Kochersberger, K., L. D. Mitchell, and A.L. Wicks, "Structural Angular Velocity Extration Using DFT/IDFT Techniques," *Proceedings of IMAC-IX*, Vol. I, Florence Italy, April 14-18, 1991, pp. 657-663.

[43] Blevins, Robert D., *Formulas for Natural Frequency and Mode Shape*, Krieger Publishing Company, Malabar, FL, 1995, pp. 252-264.

[44] Lessia, Arthur, *Vibration of Plates*, Acoustical Society of America, Sewickley, PA, 1993, Chap 4.

[45] Lloyd, P., and Redwood, M., "Finite-Difference Method for the Investigation of the Vibrations of Solids and the Evaluation of the Equivalent-Circuit Characteristics of Piezoelectric Resonators," *The Journal of the Acoustical Society of America*, Vol. 39, No. 2, 1966, pp. 347-361

[46] Anonymous, Kistler Instrument Coporation, Technical Bulletin: Type 8832 Translational-Angular PiezoBEAM (TAP) System, Amherst, NY

[47] Inslako, Mike, Personal Communication via fax and phone, Kistler Instrument Corporation, December 2-4, 1994.

Appendix

Included here is a M-file that is used to make an array periodic about one direction and take the derivative with respect to that direction and return the results. This file is include so others may find it easy to repeat the MATLAB® routine to do just that.

```
function [dWdx] = dWdft(W,lenx,leny,pctkeep)
%%%%%%%%%%%%%%%%%%%%%%%%%%%%%%%%%%%%%%%%%%%%%%%%%%%%%%%%%%%%%%%%
%%      [dWdx] = dWdft(W,lenx,leny,pctkeep)
%%
%%      Function to take the partial derivative of a 2-D signal about one direction.  In order to take the
%%      partial derivative of a second direction, the function will accept the transpose of the matrix and
%%      output the transpose of the partial derivative.
%%
%%      W              The 2-Dimensional Velociy field
%%      lenx           Spatial spacing in the x-direction (the direction of the partial derivative)
%%      leny           Spatial spacing in the y-direction
%%      pctkeep        Percent of spatial frequencies to keep expressed as a fraction
%%
%%      Written by James R DeVlaminck 07-16-2001
%%
%%%%%%%%%%%%%%%%%%%%%%%%%%%%%%%%%%%%%%%%%%%%%%%%%%%%%%%%%%%%%%%%

WW=W;   %%  Keep original data unmodified for diagnostic reasons

%%%%%     Shear the data in row direction to obtain zeros at each end

[m,n] = size(WW);

for j=1:m,
  slopex(j) = WW(j,n)-WW(j,1);
  for i=1:n,
    slxf(j) = WW(j,n)-WW(j,(n-1));
    WW(j,i)= WW(j,i) - (i-1)*slopex(j)/(n-1) - W(j,1);
  end
end

%%%%%     Mirror and flip the signal to make periodic

for j=1:m,
  WWW(j,1:n) = WW(j,1:n);
  WWW(j,(n+1):(2*n-2)) = - WW(j,n-1:-1:2);
  slxf2(j) = WWW(j,(n)) - WWW(j,(n-1));
end

figure   %%%% Show sheared and mirrored signal versus orginal
subplot(211),mesh(WWW)
```

```
title('Show sheared and mirrored signal versus orginal')
subplot(212),mesh(W)

figure
subplot(211),plot(W(10,1:n))
subplot(212),plot(WWW(10,1:2*n-2))

%%%%%    Perform the DFT

Wdft = fft(WWW').';

%%%%%    Derivative of IFFT

dWdx = zeros(size(WW));
Wnew = zeros(size(WW));
[M,N] = size(WWW);
dx = lenx/(n-1);

for i=1:n,
for j=1:m,
  for r=1:floor((N/2+1)*pctkeep),
    constx = 2*pi*(r-1)/N;
    dcx = sqrt(-1)*2*pi*(r-1)/N/dx;
    if r == 1,
      dWdx(j,i) = dWdx(j,i) + 1/N * Wdft(j,r) * dcx * exp(sqrt(-1)*(constx*(i-1)) );
      Wnew(j,i) = Wnew(j,i) + 1/N * Wdft(j,r) * exp(sqrt(-1)*(constx*(i-1)) );
    elseif r == (N/2+1),
      dWdx(j,i) = dWdx(j,i) + 1/N * Wdft(j,r) * dcx * exp(sqrt(-1)*(constx*(i-1)) );
      Wnew(j,i) = Wnew(j,i) + 1/N * Wdft(j,r) * exp(sqrt(-1)*(constx*(i-1)) );
    else,
      dWdx(j,i) = dWdx(j,i) + 2/N * Wdft(j,r) * dcx * exp(sqrt(-1)*(constx*(i-1)) );
      Wnew(j,i) = Wnew(j,i) + 2/N * Wdft(j,r) * exp(sqrt(-1)*(constx*(i-1)) );
    end
  end
end
end

%%%%%    Must add in the slope to complete the derivative

for j=1:m,
  for i=1:n,
    Wnew(j,i) = Wnew(j,i) + (i-1)*slopex(j)/(n-1);
    dWdx(j,i) = dWdx(j,i) + slopex(j)/lenx;
  end
end


dWdx=real(dWdx);
```

Vita

James R. DeVlaminck II was born on November 25, 1971, to James and Shirley DeVlaminck in the city of Mt. Clemens, Michigan. In June of 1989, James graduated valedictorian and class president from New Haven High School. In September of 1989, he began studies at frosty Michigan Technological University, Houghton, Michigan, working toward his Bachelor of Science degree in Mechanical Engineering. While there, he served as the Junior class representative to the Undergraduate Student Government. He tutored students in the area of Statics and Dynamics during his junior and senior years. He also spent summers gainfully employed at various locations and divisions of General Motors. The summer following his junior year he happily married Kellie Denise Heckman on July 25, 1992. In May 1993, he completed the requirements for the degree of Bachelor of Science in Mechanical Engineering at Michigan Tech.

James continued his education August of 1993 at Virginia Polytechnic Institute and State University (VPI&SU) towards a Masters Degree in Mechanical Engineering. On February 17, 1994, James and Kellie proudly brought into this world their beautiful, healthy daughter Kelsie Elizabeth DeVlaminck. In February 1995, James regretfully left VPI & SU to pursue a career as a sound and vibration engineer at Whirlpool Corporation. Since that time he fathered two more healthy active boys, James III (March 14, 1995) and Jacob Ryan (August 24, 1997) . In July of 2001, James will have completed the requirements for the degree of Master of Science in Mechanical Engineering at Virginia Tech.